recent history of a stay in sub-Saharan Africa is usually challenging. Since there were no systemic findings characteristic of a specific tropical disease in this patient, we were obliged to rely on epidemiologic and brain MRI features to establish the provisional diagnosis. The patient's final diagnosis was made by PCR assay using a brain specimen from the surgical excision. Although the prevalence of central nervous system (CNS) invasion in schistosomal infection has been considered to be low (20), CNS involvement in *S. haematobium* infection may be underdiagnosed. An autopsy study in Africa showed that over half of patients infected with *S. haematobium* in the bladder had brain lesions (8). Another pathological study in Africa has found scattered ova of *S. haematobium* or *S. mansoni* in the brain at autopsy in over a quarter of 150 unselected cadavers (1).

Among 22 previous cases of cerebral schistosomiasis due to *S. haematobium*, 7 cases were diagnosed by ovum excretion in urine or feces (15, 23), and 15 cases were diagnosed by immunological testing (18). However, the detailed mechanism of egg deposition in the brain remains unknown. The presence of egg deposits may reflect either an aberrant migration of worms or the embolization of eggs from a remote location (19, 27). In this case, no worms were detected in the brain specimen, and portal hypertension or liver cirrhosis, which could increase the possibility of worm migration to the CNS (26), was not observed. These findings suggest that cerebral schistosomiasis in this case was caused by translocated eggs from a remote location rather than by eggs from ectopically parasitizing adult worms in the brain.

Diagnosing cerebral schistosomiasis can be difficult, since neurological symptoms and radiological findings are nonspecific. In some reported cases of neuroschistosomiasis, brain tumors, such as meningioma and glioma, had been suspected initially (2, 13, 23). Moreover, as in the present case, patients with cerebral schistosomiasis may have no clinical evidence of systemic disease (21, 28). The presence of parasite ova in the urine and/or stool can be detected in only 40 to 50% of neuroschistosomiasis patients (7). Antibody-based assays are quite sensitive but cannot distinguish a history of exposure from acute infection; they can also cross-react with other helminths (3, 9), such as *T. solium* (12). In our patient, the elevated IgG antibody of *Spirometra erinacei* screened by the commercial ELISA led to a presumptive diagnosis of cerebral sparganosis, which in radiological findings mimics cerebral schistosomiasis. The further ELISA performed after histopathological analysis of the brain specimen revealed that IgG antibody titers of *S. haematobium*, *S. mansoni*, and *Spirometra erinacei* were increased. An elaborate examination to screen the infectious focus outside the brain could not detect any abnormality. We then tried to detect the parasite DNA directly from the brain specimen and successfully amplified *S. haematobium* DNA by PCR assay (Fig. 3). These results strongly suggest that PCR assays are helpful means of confirming the results of serum ELISAs for schistosomiasis. Identification and differentiation of human schistosomiasis by PCR in the laboratory setting (16) and in clinical specimens (24, 26) have been reported.

Praziquantel, a pyrazinoisoquinoline derivative, is the mainstay of the treatment for human schistosomiasis. While the standard regimen for chronic systemic schistosomiasis is 40 to 60 mg/kg of praziquantel in divided doses for 1 day, as described in the Centers for Disease Control and Prevention database (http://www.cdc.gov/parasites/schistosomiasis/health_professionals/index.html), the length of the treatment for cerebral schistosomiasis has not been clearly established (4). To reduce the severity of the inflammatory reaction in the brain parenchyma, corticosteroids are commonly used for CNS invasion. Repeated courses of praziquantel and corticosteroids may be required to reduce neurological symptoms in a severe case (13). Our patient responded well to 40 mg/kg of praziquantel in two divided doses for a total of 3 days after surgical excision of the nodules (5, 6).

In conclusion, we report the first case of cerebral schistosomiasis due to *S. haematobium* that was diagnosed by molecular methods. We successfully treated the patient with surgical excision and oral praziquantel. PCR assay is a promising method for definitive diagnosis and species identification of cerebral schistosomiasis when *Schistosoma* ova in urine and/or stool are absent.

We are grateful to Nobuaki Akao for support of the diagnosis, and Yukari Horie, Naoki Oyaizu, and Haruo Onoda for their excellent technical assistance. We thank Kei Ouchi for his comments on drafts of the manuscript.

REFERENCES

1. **Alves, W.** 1958. The distribution of schistosoma eggs in human tissues. Bull. World Health Organ. **18:**1092–1097.
2. **Braga, B. P., L. B. da Costa Junior, and J. R. Lambertucci.** 2003. Magnetic resonance imaging of cerebellar schistosomiasis mansoni. Rev. Soc. Bras Med. Trop. **36:**635–636.
3. **Carod-Artal, F. J.** 2008. Neurological complications of Schistosoma infection. Trans. R. Soc. Trop. Med. Hyg. **102:**107–116.
4. **Carod-Artal, F. J.** 2010. Neuroschistosomiasis. Expert Rev. Anti Infect. Ther. **8:**1307–1318.
5. **Chen, A. W., M. H. Alam, J. M. Williamson, and L. A. Brawn.** 2006. An unusually late presentation of neuroschistosomiasis. J. Infect. **53:**e155–e158.
6. **Doherty, J. F., A. H. Moody, and S. G. Wright.** 1996. Katayama fever: an acute manifestation of schistosomiasis. BMJ **313:**1071–1072.
7. **Ferrari, T. C., P. R. Moreira, and A. S. Cunha.** 2004. Spinal cord schistosomiasis: a prospective study of 63 cases emphasizing clinical and therapeutic aspects. J. Clin. Neurosci. **11:**246–253.
8. **Gelfand, M.** 1950. Schistosomiasis in South Central Africa, p. 194–202. Post Graduate Press, Capetown, South Africa.
9. **Gryseels, B., K. Polman, J. Clerinx, and L. Kestens.** 2006. Human schistosomiasis. Lancet **368:**1106–1118.
10. **Hamburger, J., Na He, I. Abbasi, R. M. Ramzy, J. Jourdane, and A. Ruppel.** 2001. Polymerase chain reaction assay based on a highly repeated sequence of Schistosoma haematobium: a potential tool for monitoring schistosome-infested water. Am. J. Trop. Med. Hyg. **65:**907–911.
11. **Hamburger, J., Y. X. Xu, R. M. Ramzy, J. Jourdane, and A. Ruppel.** 1998. Development and laboratory evaluation of a polymerase chain reaction for monitoring Schistosoma mansoni infestation of water. Am. J. Trop. Med. Hyg. **59:**468–473.
12. **Handali, S., et al.** 2010. Multiantigen print immunoassay for comparison of diagnostic antigens for Taenia solium cysticercosis and taeniasis. Clin. Vaccine Immunol. **17:**68–72.
13. **Houston, S., et al.** 2004. First report of Schistosoma mekongi infection with brain involvement. Clin. Infect. Dis. **38:**e1–e6.
14. **Ishii, H., et al.** 2001. A rare case of eosinophilic pleuritis due to sparganosis. Intern. Med. **40:**783–785.
15. **Jaureguiberry, S., et al.** 2007. Acute neuroschistosomiasis: two cases associated with cerebral vasculitis. Am. J. Trop. Med. Hyg. **76:**964–966.
16. **Kato-Hayashi, N., et al.** 2010. Identification and differentiation of human schistosomes by polymerase chain reaction. Exp. Parasitol. **124:**325–329.
17. **Kim, D. G., et al.** 1996. Cerebral sparganosis: clinical manifestations, treatment, and outcome. J. Neurosurg. **85:**1066–1071.
18. **Liu, H. Q., X. Y. Feng, Z. W. Yao, and H. P. Sun.** 2006. Characteristic magnetic resonance enhancement pattern in cerebral schistosomiasis. Chin. Med. Sci. J. **21:**223–227.
19. **Liu, L. X.** 1993. Spinal and cerebral schistosomiasis. Semin. Neurol. **13:**189–200.
20. **Maguire, J. H.** 2010. Trematodes (schistosomes and other flukes), p. 3595–3605. *In* G. L. Mandell, J. E. Bennett, and R. Dolin (ed.), Mandell, Douglas, and Bennett's principle and practice of infectious diseases, 7th ed., vol. 2. Churchill Livingstone, Philadelphia, PA.
21. **Massachusetts General Hospital.** 2001. Case records of the Massachusetts

General Hospital. Weekly clinicopathological exercises. Case 21-2001. A 31-year-old man with an apparent seizure and a mass in the right parietal lobe. N. Engl. J. Med. **345:**126–131.
22. **Nawa, Y.** 1997. Histopathological and immunological diagnosis for parasitic zoonoses, p. 39–52. *In* H. Ishikura (ed.), Host response to international parasitic zoonoses. Springer, Tokyo, Japan.
23. **Pollner, J. H., A. Schwartz, A. Kobrine, and D. M. Parenti.** 1994. Cerebral schistosomiasis caused by Schistosoma haematobium: case report. Clin. Infect. Dis. **18:**354–357.
24. **Sandoval, N., et al.** 2006. A new PCR-based approach for the specific amplification of DNA from different Schistosoma species applicable to human urine samples. Parasitology **133:**581–587.
25. **Suzuki, T., et al.** 2006. Early detection of Schistosoma mansoni infection by touchdown PCR in a mouse model. Parasitol. Int. **55:**213–218.
26. **van Dijk, K., et al.** 2010. The potential of molecular diagnosis of cutaneous ectopic schistosomiasis. Am. J. Trop. Med. Hyg. **83:**958–959.
27. **Wang, P., et al.** 2010. Research development of the pathogenesis pathways for neuroschistosomiasis. Neurosci. Bull. **26:**168–174.
28. **Zhou, J., et al.** 2009. Cerebral schistosomiasis japonica without gastrointestinal system involvement. Surg. Neurol. **71:**481–486.

Free Radical Biology & Medicine 51 (2011) 773–779

Contents lists available at ScienceDirect

Free Radical Biology & Medicine

journal homepage: www.elsevier.com/locate/freeradbiomed

Inhibition of surgical trauma-enhanced peritoneal dissemination of tumor cells by human catalase derivatives in mice

Chika Nishizaki [a], Makiya Nishikawa [a,*], Tomoya Yata [a], Toshiyuki Yamada [a], Yuki Takahashi [a], Masahide Oku [b], Hiroya Yurimoto [b], Yasuyoshi Sakai [b], Kenji Nakanishi [c], Yoshinobu Takakura [a]

[a] Department of Biopharmaceutics and Drug Metabolism, Graduate School of Pharmaceutical Sciences, Kyoto University, Sakyo-ku, Kyoto 606–8501, Japan
[b] Division of Applied Life Sciences, Graduate School of Agriculture, Kyoto University, Sakyo-ku, Kyoto 606–8502, Japan
[c] Department of Immunology and Medical Zoology, Hyogo College of Medicine, Nishinomiya, Hyogo 663–8501, Japan

ARTICLE INFO

Article history:
Received 6 April 2011
Revised 19 May 2011
Accepted 20 May 2011
Available online 27 May 2011

Keywords:
Recombinant human catalase
Surgical trauma
Tumor metastasis
Reactive oxygen species
Free radicals

ABSTRACT

Surgical trauma, which is inevitably associated with the surgical removal of cancer, has been reported to accelerate tumor metastasis. The close association of reactive oxygen species with the trauma and tumor metastasis supports the possibility of using antioxidants for the inhibition of metastasis. To inhibit surgical trauma-enhanced peritoneal dissemination, human catalase (hCAT) derivatives, i.e., hCAT–nona-arginine peptide (hCAT-R9) and hCAT–albumin-binding peptide (hCAT-ABP), were designed to increase the retention time of the antioxidant enzyme in the abdominal cavity after intraperitoneal administration. Both ^{125}I-labeled derivatives showed significantly prolonged retention in the cavity compared to ^{125}I-hCAT. Cauterization of the cecum of mice with a hot iron, an experimental model of surgical trauma, induced abdominal adhesions. In addition, cauterization followed by colon26 tumor cell inoculation increased lipid peroxidation in the cecum and mRNA expression of molecules associated with tissue repair/adhesion and inflammation in the peritoneum. hCAT derivatives significantly suppressed the increased mRNA expression. The cauterization also increased the number of tumor cells in the abdominal organs, and the number was significantly reduced by hCAT-R9 or hCAT-ABP. These results indicate that hCAT-R9 and hCAT-ABP, both of which have a long retention time in the peritoneal cavity, can be effective at inhibiting surgery-induced peritoneal metastasis.

Much effort has been made to reduce the recurrence and metastasis of cancer after its surgical removal. However, recurrence and metastasis remain the major cause of cancer death [1]. Surgical removal, which is a pivotal treatment for most solid cancers, including gastrointestinal carcinoma and ovarian carcinoma, has been suspected to facilitate cancer cell metastasis. This speculation has been supported by several animal studies, in which surgical stress aggravated tumor metastasis [2–5]. Although the mechanism whereby surgical stress enhances tumor metastasis is not fully understood, surgery-induced inflammation and subsequent wound healing have been considered to contribute to the facilitation of tumor metastasis [6,7]. In the processes of inflammation and wound healing, the expression of a variety of proinflammatory cytokines and growth factors is upregulated, which leads to increased production of extracellular matrix (ECM)[1] components. Spilled tumor cells easily adhere to abdominal organs because of abundant ECM components and upregulated adhesion molecules. Then, the environment, being rich with growth and angiogenic factors, accelerates the proliferation of tumor cells and the formation of new blood vessels to form metastases. Thus, most, if not all, the steps of metastatic tumor growth, such as adhesion to the peritoneum and abdominal organs, proliferation, and angiogenesis, are promoted by surgical trauma and the subsequent tissue repair.

Reactive oxygen species (ROS) are involved in both inflammation and tissue repair, and sublethal levels of ROS have been reported to aggravate tumor metastasis [8]. Therefore, eliminating ROS generated by surgical removal of a primary tumor could be an effective approach to inhibiting postoperative peritoneal metastasis. Among ROS, hydrogen peroxide has the longest half-life and plays a role as a second messenger that directly activates several transcription factors, including hypoxia-inducible factor-1 [9] and nuclear factor κB [10].

Catalase is the enzyme that catalyzes the decomposition of hydrogen peroxide. Recent studies in experimental peritoneal metastasis mouse models have reported that tumor metastasis is efficiently inhibited by catalase derivatives with prolonged retention in the peritoneal cavity [11,12]. We have developed cytophilic

Abbreviations: hCAT, human catalase; hCAT-R9, human catalase fused with RRRRRRRRR; hCAT-ABP, human catalase fused with albumin-binding peptide; ^{125}I-hCAT, ^{125}I-labeled human catalase; ECM, extracellular matrix; ROS, reactive oxygen species; ABP, albumin-binding peptide; CD, circular dichroism; PAI-1, plasminogen activator inhibitor-1; TGF-β1, transforming growth factor-β1; ICAM-1, intracellular adhesion molecule-1; VEGF, vascular endothelium growth factor; TNF-α, tissue necrosis factor-α; GAPDH, glyceraldehyde-3-phosphate dehydrogenase; RT-PCR, reverse transcription–polymerase chain reaction; MDA, malondialdehyde.

* Corresponding author. Fax: +81 75 753 4614.
E-mail address: makiya@pharm.kyoto-u.ac.jp (M. Nishikawa).

0891-5849/$ – see front matter © 2011 Elsevier Inc. All rights reserved.
doi:10.1016/j.freeradbiomed.2011.05.025

derivatives of human catalase (hCAT) by fusing nona-arginine peptide (R9) or three repeats of arginine–glycine–aspartic acid and found that they were effective at inhibiting the adhesion of tumor cells to mouse aortic endothelial cells [13].

These results suggest the possibility that hCAT derivatives are effective at inhibiting surgery-induced tissue adhesion and tumor metastasis. However, a lack of appropriate experimental models of surgical trauma has made it difficult to evaluate this hypothesis. Therefore, in this study, a new surgery-induced abdominal adhesion model was developed in mice and used to evaluate the effects of hCAT derivatives on surgery-induced inflammation and peritoneal metastasis. In addition to hCAT and hCAT-R9, hCAT fused with an albumin-binding peptide (ABP) [14] was designed as another novel derivative with a long retention in the peritoneal cavity through binding to exuded serum albumin. The properties of hCAT-ABP were initially examined and the effects of hCAT derivatives on surgery-induced peritoneal metastasis of tumor cells were investigated in our surgery-induced abdominal adhesion model.

Materials and methods

Chemicals

Roswell Park Memorial Institute (RPMI) 1640 medium and Hanks' balanced salt solution (HBSS) were obtained from Nissui Pharmaceutical (Tokyo, Japan). Fetal bovine serum (FBS) was obtained from GIBCO–Invitrogen (Carlsbad, CA, USA). $Na^{125}I$ aqueous solution in 0.1 M NaOH (NEZ033, 370 MBq/ml) was purchased from PerkinElmer Life Sciences (Boston, MA, USA). Mouse and human serum albumin and bovine immunoglobulin G were purchased from Sigma–Aldrich Japan (Tokyo, Japan). All other chemicals were of the highest grade commercially available.

Animals

Male Institute for Cancer Research (ICR) mice (4 weeks of age), male BALB/c mice (4 weeks of age), and male C57BL/6 mice (4 weeks of age) were purchased from Japan SLC, Inc. (Shizuoka, Japan), and maintained on a standard food and water diet under conventional housing conditions. The protocols for the animal experiments were approved by the Animal Experimentation Committee of the Graduate School of Pharmaceutical Sciences of Kyoto University.

Cell cultures

Colon26/Luc, a clone of murine colon carcinoma colon26 that stably expresses firefly luciferase [11], was grown in RPMI 1640 medium supplemented with 10% heat-inactivated FBS, 0.15% $NaHCO_3$, 100 units/ml penicillin, and 100 μg/ml streptomycin at 37°C in humidified air containing 5% CO_2. B16-BL6 cells, clones of murine melanoma, were grown as reported previously [11].

Preparation of human catalase derivatives

hCAT and hCAT-R9 were obtained as reported previously [13]. hCAT-ABP was designed by replacing the C-terminal 11 amino acid residues (SHLAAREKANL) of hCAT with an ABP having the amino acid sequence GGGSQRLMEDICLPRWGCLWEDDF [14]. A double-stranded oligonucleotide corresponding to ABP (forward sequence, 5′-GGAGGAGGTAGTCAAAGATTGATGGAAGACATTTGCTTGCCCAGATGGGGATGCTTGTGGGAAGACGACTTC-3′) was obtained by PCR amplification with two oligonucleotides (5′-TCCCCGCGGGAGGAGGTAGTCAAAGATTGATGGAAGACATTTGCTTGCCCAGATGG-3′ and 5′-GCTCTAGAGCTCAGAAGTCGTCTTCCCACAAGCATCCCCATCTGGGCAAGCAAATGTC-3′) purchased from GIBCO–Invitrogen. The PCR fragment was digested with *Sac*II and *Xba*I and inserted into the *Sac*II–*Spe*I site of hCAT expressing the pNT40 vector to construct the hCAT-ABP-expressing plasmid vector. hCAT-ABP was obtained similar to hCAT and hCAT-R9 using a *Pichia pastoris* expression system. Recombinant catalase derivatives were purified as described previously [13], and the purity was identified by SDS–PAGE stained with Coomassie Brilliant Blue. The activity of hCAT, hCAT-R9, and hCAT-ABP was 33,800 to 37,900, 21,800 to 44,200, and 9000 to 68,300 units/mg protein, respectively [15]. The differences in the activity would be due to the denaturation of the samples during the expression and/or purification processes. In vivo effects of hCAT derivatives on mRNA expression, intra-abdominal adhesion, and dissemination of tumor cells were evaluated using hCAT derivatives with high specific enzymatic activities: 33,800, 68,300, and 21,800–40,000 for hCAT, hCAT-ABP, and hCAT-R9, respectively. The enzymes were stored in a 50% glycerol solution at −20°C until required and they were stable under these conditions for at least for 12 months. The buffer was replaced with saline by ultrafiltration for animal studies.

Measurement of circular dichroism

Circular dichroism (CD) spectra were recorded on a Jasco-820-type spectropolarimeter (Jasco, Tokyo, Japan) at 4°C. For calculation of the mean residue ellipticity (θ), the molecular mass of the hCAT derivatives was assumed to be 240 kDa [16]. Far-UV (wavelength 200–250 nm) CD spectra were recorded at a protein concentration of 0.2 mg/ml in a 50% glycerol solution.

Albumin-affinity assay

The binding affinity of hCAT derivatives to albumin or other proteins was determined as described previously [17]. Briefly, 2 μg mouse serum albumin, human serum albumin, or bovine immunoglobulin G was added to each well of 96-well plates at a volume of 100 μl/well and incubated overnight at 4°C. The plates were blocked with phosphate-buffered saline (PBS; pH 7.0) containing 0.5% ovalbumin and 0.05% Tween 20 for 60 min at room temperature. hCAT or hCAT-ABP serially diluted in PBS (pH 7.0) was added to the immobilized albumin at a volume of 100 μl/well and incubated for 90 min at 25°C. Unbound hCAT derivatives were removed by washing wells with PBS containing 0.05% Tween 20. Then, rabbit anti-catalase antibody was added to each well and incubated for 60 min at room temperature. Excess antibody was removed by washing, and goat anti-rabbit Fab′2-horseradish peroxidase (HRP) was added and incubated for 60 min at 25°C. Bound HRP was detected with a tetramethylbenzidine/hydrogen peroxide solution. After 20 min, the reaction was quenched by the addition of 1 M phosphoric acid. The absorbance at 450 nm was read at a reference wavelength of 590 nm.

^{125}I labeling

hCAT derivatives were radiolabeled with ^{125}I using the chloramine-T method [18]. A 90-μl volume of sample solution (200 μg/ml) was mixed with 10 μl 0.5 M phosphate buffer (pH 7.4) and 3 μl $Na^{125}I$ solution. Then, 10 μl chloramine-T diluted in 0.1 M phosphate buffer (pH 7.4) was added, and the mixture was vortexed for 30 s and incubated for 10 min at room temperature. Finally, 10 μl sodium metabisulfite solution (2.5 mM) was added and vortexed for 30 s. The solution was applied to a PD-10 column (GE Healthcare, Tokyo, Japan) and eluted with 0.25 M phosphate buffer (pH 7.4) containing 0.2% bovine serum albumin. The eluent was collected in plastic tubes and the radioactivity was measured in a well-type NaI-scintillation counter (ARC-500; Aloka, Tokyo, Japan). Appropriate fractions were taken and stored at −20°C until required for use.

Tissue distribution of ^{125}I-hCAT derivatives after intraperitoneal injection

Each ^{125}I-labeled hCAT derivative was injected intraperitoneally into male ICR mice at a dose of 0.5 mg/kg mouse. At appropriate intervals after injection, ascitic fluid was collected by injecting 5 ml PBS. The peritoneum, liver, kidneys, and gastrointestinal tract were collected and washed with saline. The radioactivity of the tissue samples was counted as described above.

Surgical trauma mouse model

Male BALB/c mice or male C57BL/6 mice were anesthetized with isoflurane. An approximately 10-mm-long anterior midline incision was made through the abdominal wall and peritoneum. The cecum was gently isolated from the abdominal cavity and cauterized for 1 s using an electrical soldering iron (Mypen Alpha; HAKKO, Osaka, Japan). The cecum was returned to its normal position and the incision was closed with silk sutures. Administration of hCAT derivatives (500 units in 0.1 ml saline) was carried out immediately after closure by intraperitoneal injection. Five minutes after the surgery, 1×10^5 colon26/Luc cells (BALB/c mice) or B16-BL6 cells (C57BL/6 mice) in 0.1 ml HBSS were inoculated into the cavity by intraperitoneal injection.

Measurement of luciferase activity

At 3 days after inoculation of tumor cells, the peritoneum, liver, gastrointestinal tract, and greater omentum were removed. The tissues were homogenized in a lysis buffer (0.05% Triton X-100, 0.1 M Tris, pH 7.8) followed by centrifugation at 13,000g for 10 min. Then 10 μl of the supernatant was mixed with 50 μl of luciferase assay buffer (Picagene; Toyo Ink, Tokyo, Japan) and the light produced was measured in a luminometer (Lumat LB 9507; EG&G Berthold, Bad Wildbad, Germany).

mRNA quantification

Total RNA was isolated using Sepasol RNAI Super (Nacalai Tesque, Kyoto, Japan). The changes in the mRNA level of plasminogen activator inhibitor-1 (PAI-1), transforming growth factor-β1 (TGF-β1), intracellular adhesion molecule-1 (ICAM-1), vascular endothelium growth factor (VEGF), and tissue necrosis factor-α (TNF-α) were examined using a real-time polymerase chain reaction (RT-PCR). Reverse transcription was performed using a ReverTra Ace qPCR RT kit (Toyobo, Osaka, Japan). For quantitative analysis of mRNA expression, RT-PCR was carried out with total RNA using a Light Cycler instrument (Roche Diagnostics, Basel, Switzerland). The oligonucleotide primers used for amplification were as follows: PAI-1, forward, 5′-TCAGCCCTTGCTTGCCTCAT-3′, and reverse, 5′-GCATAGCCAGCACCGAGGA-3′; TGF-β1, forward, 5′-TTGCTTCAGCTCCACAGAGA-3′, and reverse, 5′-TGGTTGTAGAGGGCAAGGAC-3′; ICAM-1, forward, 5′-GGGAATGTCACCAGGAAT-3′, and reverse, 5′-TCCTGAGCCTTCTGTAACTTG-3′; VEGF, forward, 5′-TTCAGAGCGGAGAAAGCATT-3′, and reverse, 5′-GAGGAGGCTCCTTCCTGC-3′; TNF-α, forward, 5′-AGCCGATGGGTTGTACCTTGTCTA-3′, and reverse, 5′-TGAGATAGCAAATCGGCTGACGGT-3′; GAPDH, forward, 5′-CTGCCAAGTATGATGACATCAACAA-3′, and reverse, 5′-ACCAGGAAATGAGCTTGACA-3′. Amplified products were detected online via intercalation of the fluorescent dye SYBR green (LightCycler-FastStart DNA Master SYBR Green I kit; Roche Diagnostics). The mRNA expression of the target genes of interest was normalized to the mRNA level of GAPDH.

Measurement of lipid peroxides

The isolated cecum was homogenized in 1.15% KCl solution and centrifuged at 4000g for 10 min, and 200 μl of the supernatant was mixed with 25 μl of 2,6-di-*tert*-butyl-4-methylphenol (5 mM in ethanol) and 200 μl of orthophosphoric acid (0.2 M). Then, 25 μl of 2-thiobarbituric acid (TBA) reagent (0.11 M TBA in 0.1 M NaOH) was added, followed by vortexing for 10 s to allow reaction with malondialdehyde (MDA). After incubation for 45 min at 90°C, thiobarbituric acid-reactive substances (TBARS) were extracted with 0.5 ml *n*-butanol. Then, the TBARS-derived fluorescence was measured in a multilabel counter (excitation at 530 nm, emission at 560 nm, Wallac 1420 ARVO MX-2; PerkinElmer Life Sciences). Separately, the protein concentration of the supernatant was assayed using a BCA protein assay kit (Pierce, Rockford, IL, USA). The TBARS values were normalized with regard to the protein content.

Statistical analysis

Differences were statistically evaluated by one-way analysis of variance followed by Fisher's LSD for multiple comparisons and by Student's *t* test for two groups. *P* values of less than 0.05 were considered statistically significant.

Results

Properties of human catalase derivatives

The properties of hCAT-R9 have already been reported [13]. The SDS–PAGE analysis showed a single band of about 60 kDa (Fig. 1A), which was comparable with the molecular weight of the hCAT monomer and consistent with the estimated molecular weight of hCAT-ABP (about 61 kDa). Fig. 1B shows the far-UV CD spectra of hCAT and hCAT-ABP. There was no significant difference in the spectra of hCAT and hCAT-ABP, indicating that the fusion of ABP to the C-terminal of human catalase hardly altered the secondary structure. hCAT-ABP was bound to immobilized mouse serum albumin, whereas hCAT was not (Fig. 1C). The binding of hCAT-ABP to the albumin was marked compared with the binding to human serum albumin or bovine immunoglobulin G (Fig. 1D). hCAT-R9 was also bound to immobilized mouse serum albumin, but its binding affinity was lower than that of hCAT-ABP. Its affinity for mouse serum albumin was comparable with that to human serum albumin or immunoglobulin G, suggesting that hCAT-R9 weakly and nonspecifically binds to negatively charged proteins (data not shown).

Retention of human catalase derivatives in the abdomen

The radioactivity in the ascitic fluid, peritoneum, greater omentum, liver, kidneys, and gastrointestinal tract was summed and used as an indicator of the retention of ^{125}I-hCAT derivatives in the abdomen after intraperitoneal injection. Fig. 2A shows the time course of radioactivity in the abdomen of mice after intraperitoneal injection of ^{125}I-hCAT derivatives. About 67% of the radioactivity remained 1 h after injection of ^{125}I-hCAT-R9, which was significantly higher than that after injection of ^{125}I-hCAT or ^{125}I-hCAT-ABP. A high distribution of hCAT derivatives was observed in the gastrointestinal tract and ascitic fluid (Fig. 2B). At 8 h after injection, significantly higher radioactivity was detected in the gastrointestinal tract after injection of ^{125}I-hCAT-R9 or ^{125}I-hCAT-ABP than after ^{125}I-hCAT (Fig. 2C). There was no significant radioactivity detected in the thyroid, suggesting that the radioactivity reflects the distribution of ^{125}I-hCAT derivatives (data not shown).

Abdominal changes induced by cauterization and tumor inoculation

The cauterization induced intra-abdominal adhesions among the cecum, peritoneum, gastrointestinal tract, and adipose tissue (Supplemental Figs. A and B). To examine the overproduction of ROS by surgical treatment, the level of MDA, a marker for lipid peroxidation,

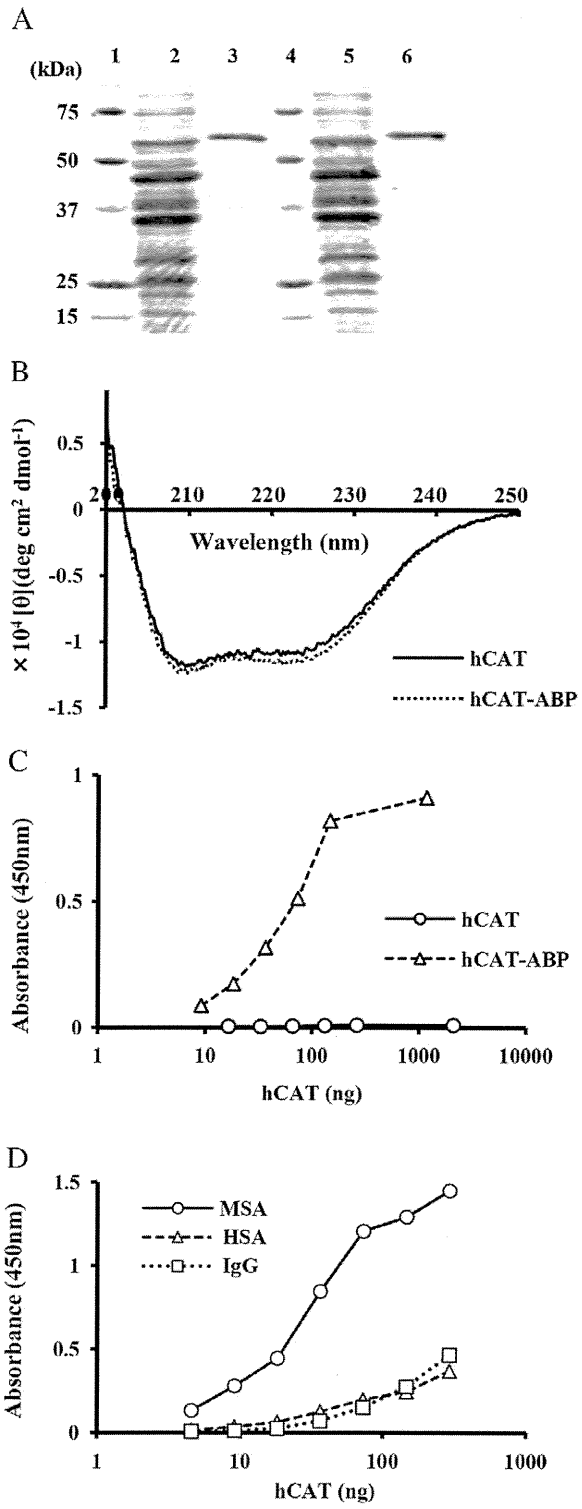

Fig. 1. Characteristics of hCAT derivatives. (A) SDS–PAGE analysis of hCAT derivatives stained with Coomassie Brilliant Blue. Lanes 1 and 4, Precision Protein unstained marker (Bio-Rad); lanes 2 and 5, crude hCAT (lane 2) and hCAT-ABP (lane 5); lanes 3 and 6; hCAT (lane 3) and hCAT-ABP (lane 6) purified using glutathione–Sepharose column. (B) Far-UV CD spectra of hCAT derivatives. The protein concentration was 0.2 mg/ml in 50% glycerol buffer. (C) Binding of hCAT derivatives to immobilized mouse serum albumin. (D) Binding of hCAT-ABP to immobilized mouse serum albumin, human serum albumin, or bovine immunoglobulin G. Key: MSA, mouse serum albumin; HSA, human serum albumin; IgG, bovine immunoglobulin G.

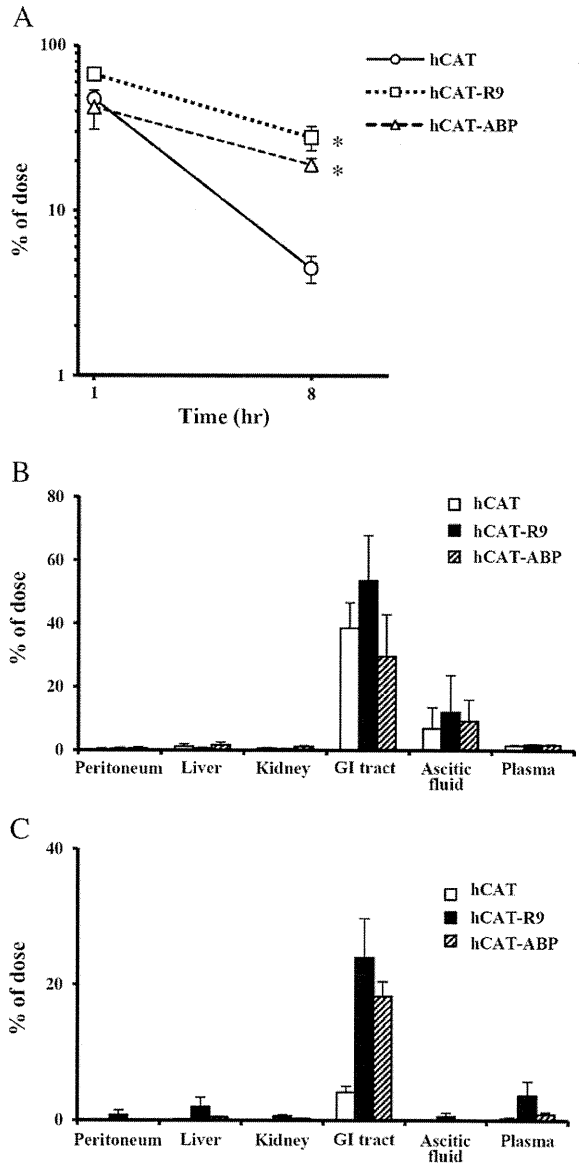

Fig. 2. Disappearance of radioactivity after intraperitoneal injection of ^{125}I-hCAT derivatives. (A) Time course of the total ^{125}I radioactivity in the abdominal organs and ascitic fluid of mice after intraperitoneal injection of ^{125}I-hCAT, ^{125}I-hCAT-R9, and ^{125}I-hCAT-ABP (0.5 mg/kg wt). Results are expressed as the means ± SE of four mice. *$P < 0.05$ compared with ^{125}I-hCAT group at the same time point. (B, C) The tissue distribution of ^{125}I radioactivity at (B) 1 or (C) 8 h after intraperitoneal injection of ^{125}I-hCAT derivatives. Results are expressed as the means ± SE of four mice. *$P < 0.05$ compared with the ^{125}I-hCAT group.

in the cecum was measured on postoperative day 1. The MDA level of the surgery group was about five times higher than that in the nonsurgery group (Fig. 3A). The mRNA expression levels of PAI-1, TGF-β1, ICAM-1, VEGF, and TNF-α in the peritoneum were significantly increased by the surgical treatment (Fig. 3B), suggesting that inflammation and wound healing took place. Intra-abdominal metastasis was markedly accelerated and widely disseminated by surgical trauma, especially in the peritoneum, the cauterized cecum, and the adhesion sites (Supplemental Figs. C–D). The total number of tumor cells increased about 12-fold on postoperative day 3 (Fig. 3C). A similar difference was also observed on postoperative day 14 (data not shown).

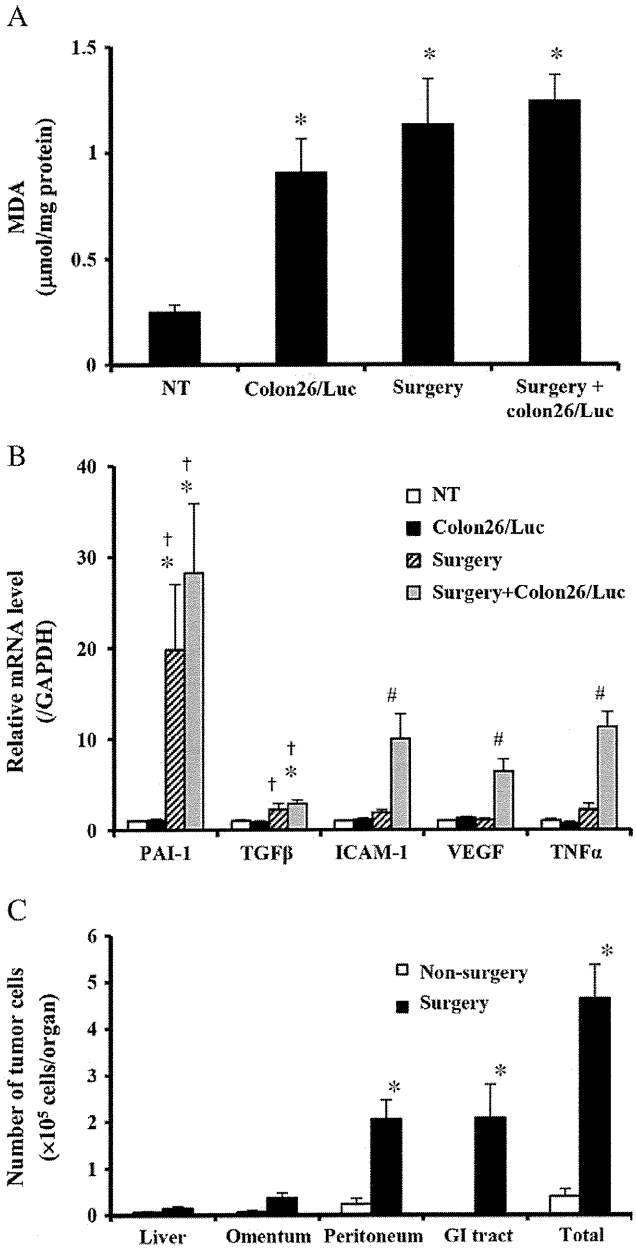

Fig. 3. Effects of surgical trauma and intraperitoneal inoculation of colon26/Luc cells. (A) The level of MDA in the cecum on postoperative day 1. Results are expressed as the mean ± SE of four mice. *$P < 0.05$, compared with the no-treatment (NT) group. (B) The mRNA expression in the peritoneum on postoperative day 1. Results are expressed as the mean ± SE of three or four mice. *$P < 0.05$ compared with the no-treatment (NT) group; †$P < 0.05$ compared with the colon26/Luc group; #$P < 0.05$ compared with the other groups. (C) The total number of colon26/Luc cells in the abdominal organs on postoperative day 3. Results are expressed as the mean ± SE of three (nonsurgery) or five (surgery) mice. *$P < 0.05$ compared with the nonsurgery group.

Effect of hCAT derivatives on mRNA expression and intra-abdominal adhesion

Fig. 4 shows the mRNA expression levels in the peritoneum on postoperative day 1. The mRNA expression levels of PAI-1, TGF-β1, ICAM-1, VEGF, and TNF-α in the peritoneum were significantly increased by the surgical treatment. The injection of any hCAT derivative at a dose of 500 units/mouse was effective at preventing the surgery-induced increase in the mRNA expression. No significant difference was observed among the groups treated with hCAT or hCAT derivatives.

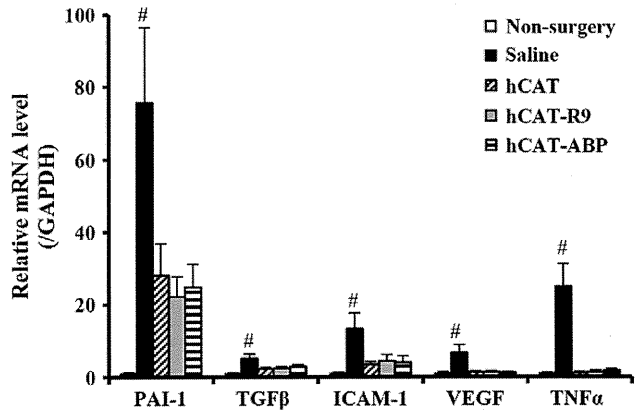

Fig. 4. Effect of hCAT derivatives on surgery-enhanced mRNA expression. The mRNA expression in the peritoneum on postoperative day 1 is shown. Results are expressed as the mean ± SE of three or four mice. #$P < 0.05$ compared with the other groups.

Inhibition of surgery-enhanced peritoneal dissemination by hCAT derivatives

Fig. 5 shows the number of colon26/Luc cells in abdominal organs 3 days after inoculation. Cauterization of the cecum significantly increased the number of colon26/Luc cells in the cecum and the peritoneum. Administration of hCAT produced a slight but not significant reduction in the number, whereas hCAT-R9 or hCAT-ABP significantly reduced it to about 41 or 28%, respectively, of that in the saline group.

Discussion

Chemically modified catalase derivatives have been reported to have a therapeutic effect on oxidative stress-induced diseases [19–23]. Despite their usefulness, they are always associated with a potential risk of heterogeneity, poor reproducibility, and reduced enzymatic activity. Instead, genetic modification techniques have been used to

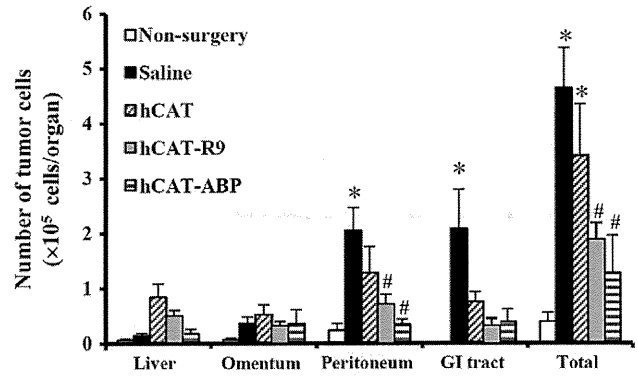

Fig. 5. Effects of hCAT derivatives on surgery-enhanced peritoneal dissemination. Colon26/Luc cells were inoculated into the peritoneal cavity (1×10^5cells) after surgery. On postoperative day 3, the liver, omentum, peritoneum, and gastrointestinal tract were isolated and the number of tumor cells was assayed. Results are expressed as the mean ± SE of three to five mice. *$P < 0.05$, compared with the nonsurgery group; #$P < 0.05$, compared with the surgery, saline group.

avoid these risks. In this study, *P. pastoris*, which has been used to express a number of proteins [24], was selected as the host to produce human catalase derivatives.

A previous study has reported that hCAT-R9 showed higher affinity for endothelial cells and a greater inhibitory effect on oxidative stress-accelerated adhesion of tumor cells in vitro than unmodified hCAT [13]. The prolonged retention of ^{125}I-hCAT-R9 suggests that it can bind to the surface of abdominal organs after intraperitoneal injection. The surface of these organs is lined with mesothelial cells, and an electrostatic interaction would be the reason for the long retention of hCAT-R9. When tissues are damaged, negatively charged basal membrane is exposed, so such a change would also become a site for hCAT-R9 binding.

Increasing the effective molecular size is another approach to prolonging the retention of hCAT in the abdominal cavity, because the systemic absorption from the cavity is a function of the size [25]. Serum albumin was selected as a partner because of its abundance and relatively large molecular size. Previous studies have reported that fusing the ABP to drugs with a short half-life improved the retention time in the blood [26]. In contrast to hCAT-R9, which exhibited a nonspecific interaction with the cell surface, hCAT-ABP could distribute to a larger area of the abdominal cavity, where it would efficiently degrade ROS. This feature might explain why hCAT-ABP exhibited somewhat higher inhibitory effects than hCAT-R9, although the difference was not statistically significant.

Surgical trauma has been suggested to be an important aggravating factor for tumor metastasis [2–5,11], but its effects on metastasis have received little attention. We developed a surgery-enhanced peritoneal metastasis mouse model according to a recent publication [27]. The tissue damage and intra-abdominal adhesions were reproducible when a fixed set of parameters were used. Therefore, this model seems to be a suitable preclinical model to investigate surgical trauma-induced tumor metastasis.

The cauterization induced a variety of changes in the abdominal organs that are typical of damaged tissues [6,7]. The increased mRNA expression of TNF-α, TGF-β1, and VEGF suggested that the damage started to heal. These factors stimulate the synthesis of ECM and the expression of adhesion molecules, such as ICAM-1. On the other hand, the increased expression of PAI-1 could suppress the degradation of ECM components. Taken together, ECM components accumulate at the wound sites and contribute to tissue repair and remodeling. This study clearly demonstrates that the surgery-induced changes significantly increase the metastatic growth of tumor cells. Therefore, it is strongly suggested that a postsurgical intraperitoneal environment is highly favorable for detached and floating tumor cells to produce metastasis.

The inhibition of mRNA expression by any hCAT derivative used (Fig. 4) indicates that the scavenging of hydrogen peroxide is a promising way of inhibiting surgery-induced mRNA overexpression. Similar trends were observed in the number of colon26/Luc cells, but only hCAT-R9 and hCAT-ABP significantly reduced it (Fig. 5). We also obtained similar results using mouse melanoma B16-BL6 cells (C. Nishizaki et al., unpublished data). A possible reason for this discrepancy is the difference in the timing of these assays: 1 and 3 days after administration for mRNA expression and the number of tumor cells, respectively. hCAT is effective at inhibiting mRNA expression at a very early time point but, because of its short retention time, it could be less effective at inhibiting metastatic tumor growth at later time points. In surgery-enhanced metastasis and recurrence, the most important process is the adhesion of tumor cells to the abdominal organs. Almost all spilled tumor cells in the cavity were reported to die within 3 days unless adhesion occurred. Therefore, hCAT derivatives can be considered to reduce the risk of cancer recurrence/metastasis, the major cause of cancer death.

There was high accumulation of ^{125}I-hCAT derivatives in the GI tract (Figs. 2B and C), whereas a significant reduction in the number of colon26/Luc cells was observed in the peritoneum of the hCAT-ABP- or hCAT-R9-treated groups (Fig. 5). This apparent discrepancy could be explained by the fact that the peritoneum is one of the typical organs in which intra-abdominal adhesions are formed (supplemental figure). In addition, the cauterization could alter the distribution of hCAT derivatives.

In conclusion, hCAT-R9 or hCAT-ABP has been found effective at inhibiting the metastasis of colon26/Luc cells after intraperitoneal injection. No significant differences were observed between hCAT-R9 and hCAT-ABP, suggesting that the retention time is important for the increased therapeutic effects of these derivatives. These results indicate that the newly developed hCAT derivatives are promising agents for inhibiting surgical trauma-enhanced peritoneal metastasis of tumor cells.

Supplementary data associated with this article can be found in the online version at doi:10.1016/j.freeradbiomed.2011.05.025.

Acknowledgment

This work is supported by a Grant-in-Aid for Scientific Research (B) from the Japan Society for the Promotion of Science.

References

[1] Simmonds, P. C.; Primrose, J. N.; Colquitt, J. L.; Garden, O. J.; Poston, G. J.; Rees, M. Surgical resection of hepatic metastases from colorectal cancer: a systematic review of published studies. *Br. J. Cancer.* **94:**982–999; 2006.
[2] Lee, J. W.; Shahzad, M. M. K.; Lin, Y. G.; Armaiz-Pena, G.; Mangala, L. S.; Han, H. D.; Kim, H. S.; Nam, E. J.; Jennings, N. B.; Halder, J.; Nick, A. M.; Stone, R. L.; Lu, C.; Lutgendorf, S. K.; Cole, S. W.; Lokshin, A. E.; Sood, A. K. Surgical stress promotes tumor growth in ovarian carcinoma. *Clin. Cancer Res.* **15:**2695–2702; 2009.
[3] Lee, S. W.; Gleason, N.; Blanco, I.; Asi, Z. K.; Whela, R. L. Higher colon cancer tumor proliferative index and lower tumor cell death rate in mice undergoing laparotomy versus insufflation. *Surg. Endosc.* **16:**36–39; 2002.
[4] Glasner, A.; Avraham, R.; Rosenne, E.; Benish, M.; Zmora, O.; Shemer, S.; Meiboom, H.; Ben-Eliyahu, S. Improving survival rates in two models of spontaneous postoperative metastasis in mice by combined administration of a β-adrenergic antagonist and a cyclooxygenase-2 inhibitor. *J. Immunol.* **184:**2449–2457; 2010.
[5] Allendorf, J. D.; Bessler, M.; Horvath, K. D.; Marvin, M. R.; Laird, D. A.; Whelan, R. L. Increased tumor establishment and growth after open vs laparoscopic bowel resection in mice. *Surg. Endosc.* **12:**1035–1038; 1998.
[6] Coussens, L. M.; Werb, Z. Inflammation and cancer. *Nature* **420:**860–867; 2002.
[7] Oosterling, S. J.; van der Bij, G. J.; van Egmond, M.; van der Sijp, J. R. Surgical trauma and peritoneal recurrence of colorectal carcinoma. *Eur. J. Surg. Oncol.* **31:** 29–37; 2005.
[8] Nishikawa, M. Reactive oxygen species in tumor metastasis. *Cancer Lett.* **266:** 53–59; 2008.
[9] Chandel, N. S.; McClintock, D. S.; Feliciano, C. E.; Wood, T. M.; Melendez, J. A.; Rodriguez, A. M.; Schumacker, P. T. Reactive oxygen species generated at mitochondrial complex III stabilize hypoxia-inducible factor-1α during hypoxia: a mechanism of O_2 sensing. *J. Biol. Chem.* **275:**25130–25138; 2000.
[10] Schmidt, K. N.; Amstad, P.; Cerutti, P.; Baeuerle, P. A. The roles of hydrogen peroxide and superoxide as messengers in the activation of transcription factor NF-κB. *Chem. Biol.* **2:**13–22; 1995.
[11] Hyoudou, K.; Nishikawa, M.; Kobayashi, Y.; Mukai, S.; Ikemura, M.; Kuramoto, Y.; Yamashita, F.; Hashida, M. Inhibition of peritoneal dissemination of tumor cells by cationized catalase in mice. *J. Controlled Release* **119:**121–127; 2007.
[12] Hyoudou, K.; Nishikawa, M.; Ikemura, M.; Kobayashi, Y.; Mendelsohn, A.; Miyazaki, N.; Tabata, Y.; Yamashita, F.; Hashida, M. Cationized catalase-loaded hydrogel for growth inhibition of peritoneally disseminated tumor cells. *J. Controlled Release* **122:**151–158; 2007.
[13] Yata, T.; Nishikawa, M.; Nishizaki, C.; Oku, M.; Yurimoto, H.; Sakai, Y.; Takakura, Y. Control of hypoxia-induced tumor cell adhesion by cytophilic human catalase. *Free Radic. Biol. Med.* **47:**1772–1778; 2009.
[14] Dennis, M. S.; Zhang, M.; Meng, Y. G.; Kadkhodayan, M.; Kirchhofer, D.; Combs, D.; Damico, L. A. Albumin binding as a general strategy for improving the pharmacokinetics of proteins. *J. Biol. Chem.* **277:**35035–35043; 2002.
[15] Shi, X. L.; Feng, M. Q.; Shi, J.; Shi, Z. H.; Zhong, J.; Zhou, P. High-level expression and purification of recombinant human catalase in *Pichia pastoris*. *Protein Expression Purif.* **54:**24–29; 2007.
[16] Ma, S. F.; Nishikawa, M.; Katsumi, H.; Yamashita, F.; Hashida, M. Liver targeting of catalase by cationization for prevention of acute liver failure in mice. *J. Controlled Release* **2:**273–282; 2006.
[17] Nguyen, A.; Reyes II, A. E.; Zhang, M.; Mcdonald, P.; Wong, W. L. T.; Damico, L. A.; Dennis, M. S. The pharmacokinetics of an albumin binding Fab (AB.Fab) can be modulated as a function of affinity for albumin. *Protein Eng. Des. Sel.* **19:**291–297; 2006.
[18] Staud, F.; Nishikawa, M.; Morimoto, K.; Takakura, Y.; Hashida, M. Disposition of radioactivity after injection of liver-targeted proteins labeled with ^{111}In or ^{125}I:

Effect of labeling on distribution and excretion of radioactivity in rats. *J. Pharm. Sci.* **88:**577–585; 1999.
[19] Nishikawa, M.; Tamada, A.; Hyoudou, K.; Umeyama, Y.; Takahashi, Y.; Kobayashi, Y.; Kumai, H.; Ishida, E.; Staud, F.; Yabe, Y.; Takakura, Y.; Yamashita, F.; Hashida, M. Inhibition of experimental hepatic metastasis by targeted delivery of catalase in mice. *Clin. Exp. Metastasis* **21:**213–221; 2004.
[20] Hyoudou, K.; Nishikawa, M.; Kobayashi, Y.; Umeyama, Y.; Yamashita, F.; Hashida, M. PEGylated catalase prevents metastatic tumor growth aggravated by tumor removal. *Free Radic. Biol. Med.* **41:**1449–1458; 2006.
[21] Ikemura, M.; Nishikawa, M.; Hyoudou, K.; Kobayashi, Y.; Yamashita, F.; Hashida, M. Improvement of insulin resistance by removal of systemic hydrogen peroxide by PEGylated catalase in obese mice. *Mol. Pharm.* **7:**2069–2076; 2010.
[22] Atochina, E. N.; Balyasnikova, I. V.; Danilov, S. M.; Granger, D. N.; Fisher, A. B.; Muzykantov, V. R. Immunotargeting of catalase to ACE or ICAM-1 protects perfused rat lungs against oxidative stress. *Am. J. Physiol.* **275:**806–817; 1998.
[23] Kozower, B. D.; Christofidou-Solomidou, M.; Sweitzer, T. D.; Muro, S.; Buerk, D. G.; Solomides, C. C.; Albelda, S. M.; Patterson, G. A.; Muzykantov, V. R. Immunotargeting of catalase to the pulmonary endothelium alleviates oxidative stress and reduces acute lung transplantation injury. *Nat. Biotechnol.* **21:**392–398; 2003.
[24] Gerngross, T. U. Advances in the production of human therapeutic proteins in yeasts and filamentous fungi. *Nat. Biotechnol.* **22:**1409–1414; 2004.
[25] Leypoldt, J. K.; Parker, H. R.; Frigon, R. P.; Henderson, L. W. Molecular size dependence of peritoneal transport. *J. Lab. Clin. Med.* **110:**207–216; 1987.
[26] Dennis, M. S.; Jin, H.; Dugger, D.; Yang, R.; McFarland, L.; Ogasawara, A.; Williams, S.; Cole, M. J.; Ross, S.; Schwall, R. Imaging tumors with an albumin-binding Fab, a novel tumor-targeting agent. *Cancer Res.* **67:**254–261; 2007.
[27] Kosaka, H.; Yoshimoto, T.; Yoshimoto, T.; Fujimoto, J.; Nakanishi, K. Interferon-γ is a therapeutic target molecule for prevention of postoperative adhesion formation. *Nat. Med.* **14:**437–441; 2008.

International Immunology, Vol. 23, No. 12, pp. 761–772
doi:10.1093/intimm/dxr087
Advance Access publication 29 October 2011

Requirement of GATA-binding protein 3 for *Il13* gene expression in IL-18-stimulated T_h1 cells

Masakiyo Nakahira and **Kenji Nakanishi**

Department of Immunology and Medical Zoology, Hyogo College of Medicine, 1-1 Mukogawa-cho, Nishinomiya, Hyogo 663-8501, Japan

Correspondence to: K. Nakanishi; E-mail: nakaken@hyo-med.ac.jp

Received 28 June 2011, *accepted* 3 October 2011

Abstract

Recent reports have revealed that $CD4^+$ T_h cell subsets have the ability to alter their gene expression pattern in response to extracellular stimuli. We previously highlighted the plasticity of T_h1 cells by demonstrating that T_h1 cells gain the capacity to produce IL-3, IL-9, IL-13 and granulocyte macrophage colony-stimulating factor in response to antigen, IL-2 and IL-18, and based on their unique function, we designated these activated T_h1 cells as 'super T_h1 cells'. However, the precise molecular mechanism underlying IL-13 production by super T_h1 cells has not been elucidated. Here, we show that the GATA-binding protein 3 (Gata3) is essentially required for *Il13* gene expression in super T_h1 cells. Gata3 is synergistically induced in T-box expressed in T-cells (T-bet)-expressing T_h1 cells when co-stimulated with anti-CD3, IL-18 and IL-4 through the activation of nuclear factor of activated T cells, nuclear factor kappa-light-chain-enhancer of activated B cells and signal transducer and activator of transcription 6, respectively. However, Gata3 induction is not satisfactory, and additional TCR or anti-CD3 signaling is prerequisite for triggering IL-13 production by Gata3 plus T-bet-expressing T_h1 cells. These findings suggest that Gata3, which is not originally expressed in T_h1 cells, alters the cytokine production profile by T_h1 cells.

Keywords: allergy, Gata3, IL-13, IL-18, T_h1 cells

Introduction

$CD4^+$ T_h cells play critical roles in controlling adaptive immune response to invading pathogens, allergens and self-antigens. Coffman and Mosmann originally classified T_h subsets into T_h1 cells and T_h2 cells based on their cytokine expression patterns. T_h1 cells produce IFN-γ, which activates macrophage and eliminates intracellular pathogens, whereas T_h2 cells produce IL-4, IL-5 and IL-13, which are crucial for IgE production, eosinophil infiltration and clearance of extracellular parasites. This T_h1/T_h2 paradigm may help elucidating the mechanism for the development of human immunological diseases. However, this paradigm cannot necessarily explain onsets of autoimmune diseases, such as experimental autoimmune encephalomyelitis and collagen-induced arthritis. Recent studies suggest contribution of T_h17 (T_h cells producing IL-17) and regulatory T cells (Treg cells) to the development of these diseases. Now, we know that there are at least four T_h cell subsets and transcription factors control T_h cell differentiation and function. T-box expressed in T-cells (T-bet), GATA-binding protein 3 (Gata3), Retinoid-Related Orphan Receptor γ t and forkhead box P3 (Foxp3) are known as the master transcription factors for T_h1, T_h2, T_h17 and Treg cells, respectively (1–4).

T_h1 cells were regarded to produce IFN-γ and IL-2. However, our previous studies revealed that, in response to IL-18, the established T_h1 cells become to produce T_h2 cytokines as well as their proper T_h1 cytokines (5–10), suggesting that T_h1 cells have plasticity. They produce T_h2 cytokines (IL-9, IL-13), granulocyte macrophage colony-stimulating factor and various chemokines that can recruit granulocytes, macrophages and lymphocytes. However, they cannot produce IL-4. We designated these T_h2 cytokines-producing T_h1 cells as 'super T_h1 cells'. Recent studies have revealed that T_h cells have plasticity in their cytokine expression profile and can be reprogrammed by master transcription factors to generate various types of immune responses (11–14). For example, Lee *et al.* (15) reported that T_h17 cells produce IFN-γ in a signal transducer and activator of transcription (Stat) 4–T-bet-dependent manner, and it is well documented that IFN-γ^+IL-17^+ T cells exist *in vivo*. Treg cells expressing Foxp3 can also produce IFN-γ in parallel with up-regulation of T-bet expression when cultured under T_h1 condition or in a T_h1-biased inflammatory environment such as *Toxoplasma gondii* infection (16, 17). Although it is supposed relatively difficult to convert the cytokine profile of T_h1 and T_h2 cells (13), Hegazy *et al.* (18) demonstrated the presence of a stable $Gata3^+$T-bet^+ cell

subset called 'T_h2+1 cells' and that T_h2 cells start to express T-bet, when stimulated with lymphocytic choriomeningitis virus (LCMV) GP_{61-68} epitope, IL-12, IFN-γ and type I interferons. However, the molecular mechanism underlying the plasticity of T_h1 cells has not been clarified.

We explored the pathological roles of super T_h1 cells *in vivo* using animal models (5, 7, 8, 10). In a bronchial asthma model, when mice bearing antigen-specific T_h1 cells were subjected to intranasal challenge with antigen and IL-18, asthma symptoms such as airway hyperresponsiveness, eosinophil infiltration and lung fibrosis were induced (5). Furthermore, we reported that exogenously administered IL-18 in a T_h1-type asthma model can mimic endogenous IL-18 released from alveolar macrophages and/or respiratory epithelial cells in response to microbial products such as lipopolysaccharide (7) or protein A from *Staphylococcus aureus* (SpA) (10), suggesting the contribution of super T_h1 cells to human bronchial asthma, which is often triggered or aggravated by bacterial or viral infection.

In addition to bronchial asthma, we demonstrated contribution of super T_h1 cells to the pathogenesis of infection-associated atopic dermatitis (AD) (8). When NC/Nga mice, which have a genetic skin defect, are treated with SDS to further weaken the skin, and subjected to topical application of SpA, they exhibited AD-like dermatitis with pruritus. We found that $CD4^+$ T cells from regional lymph nodes of mice treated with SDS/SpA for at least 7 days produced much larger amounts of IL-3 and IL-13 together with IFN-γ than those from non-treated or SDS-treated mice (8). Furthermore, keratinocytes produced IL-18 in response to SpA stimulation, implying the induction of pathological T_h1 cells, super T_h1 cells, by endogenous IL-18. Indeed, administration of anti-IL-18 antibody or *Il18* deficiency inhibited the development of AD in this mouse model.

Although we have demonstrated the involvement of super T_h1 cells in microbial infection-induced allergic diseases (9) and the capacity of human $CD4^+$ T cells to develop into super T_h1 cells (6, 10), the molecular mechanism underlying IL-13 production by super T_h1 cells remains unclear. In this report, we show that Gata3 is essentially required for *Il13* gene expression in T-bet-expressing T_h1 cells. Gata3 is optimally induced by co-stimulation with anti-CD3, IL-2 and IL-18 together with endogenous IL-4. However, Gata3 induction is not sufficient for *Il13* gene expression in T_h1 cells since anti-CD3 signaling is simultaneously needed. These findings suggest that T_h1 cells have the capacity to alter their cytokine profile in response to external stimuli.

Methods

Mice

Wild-type BALB/c and C57BL/6 mice were purchased from Charles River Laboratories Japan, Inc (Yokohama, Japan). *Stat6*-deficient (*Stat6*$^{-/-}$) mice (19) and *Il4*$^{gfp/gfp}$ mice (20) on a BALB/c background and *Il13*$^{-/-}$ mice on a C57BL/6 background (21) were described previously. All mice were housed under specific pathogen-free conditions. All experiments were performed according to the guidelines of the Institutional Animal Care Committee of Hyogo College of Medicine.

Reagents

PE-conjugated anti-mouse IL-4 (clone: 11B11; 12-7041-71; eBioscience, San Diego, CA, USA), FITC-conjugated anti-mouse IFN-γ (clone: XMG1.2; 11-7311-82; eBioscience), PE-conjugated anti-mouse IL-13 (clone: eBio13A; 12-7133-71; eBioscience), PE-conjugated anti-human/mouse Gata3 (clone: TWAJ; 12-9966-71; eBioscience), Alexa Fluor® 647 anti-mouse/human T-bet (clone: eBio4B10; 51-5825-80; eBioscience), PE-conjugated anti-mouse IL-4Rα (clone: mIL4R-M1;5552509; BD Pharmingen, San Diego, CA, USA), biotin-conjugated anti-rat IgG_1 antibody (clone: RG 11/39.4; 553890; BD Pharmingen), Streptavidin-PE (13025D; BD Pharmingen), anti-mouse IL-4Rα antibody (clone: mIL4R-M1; 552288; BD Pharmingen), rat IgG_{2a} isotype control (clone: R35-95; 553926; BD Pharmingen), FITC-conjugated anti-rat IgG_1 antibody (clone: RG 11/39.4; 553892; BD Pharmingen), anti-Gata3 (clone: HG3-31; sc-268; Santa Cruz, Santa Cruz, CA, USA), anti-mouse CD3ε (clone: 145-2C11; 100302; BioLegend, San Diego, CA, USA), anti-mouse CD28 (clone: 37.51; 102102; BioLegend), anti-mouse Fas ligand (FasL) antibody (clone: MFL3; 106608; BioLegend), Hamster IgG isotype control (clone: HTK888; 400916; BioLegend), recombinant mouse IL-12 (210-12; PEPROTECH, Rocky Hill, NJ, USA), recombinant mouse IL-13 (210-13; PEPROTECH), recombinant human IL-2 (200-02; PEPROTECH), recombinant mouse IL-4 (404-ML-010; R&D Systems, Minneapolis, MN, USA), FITC-conjugated anti-mouse IL-18Rα (clone: 112614; FAB1216F; R&D Systems), recombinant mouse IL-18 (B004-2; MBL, Nagoya, Japan), nuclear factor of activated T cells (NFAT) inhibitor (480401; Calbiochem, Darmstadt, Germany) and nuclear factor kappa-light-chain-enhancer of activated B cells (NF-κB) inhibitor [ammonium pyrrolidinedithiocarbamate (APDC); P8765; Sigma, St Louis, MO, USA] were purchased from the indicated companies. Anti-mouse IL-18Rα antibody (clone: Y38) was kindly given from Hayashibara Biochemical Laboratories (Okayama, Japan).

In vitro T_h cell differentiation and re-stimulation of T_h cells

Murine $CD4^+CD62L^{high}$ naive $CD4^+$ T cells were sorted by FACSAria (Becton Dickinson). Naive $CD4^+$ T cells were stimulated with plate-bound anti-CD3ε mAb (clone: 145-2C11, 1 μg ml^{-1} for coating) at 5×10^5 cells per well in the presence of 1 μg ml^{-1} anti-CD28 mAb (clone: 37.51) and 100 U ml^{-1} recombinant human IL-2 in a 48-well plate (0.5 ml per well) for 3 days. For T_h1 differentiation, murine IL-12 (10 ng ml^{-1}) and anti-mouse IL-4 (clone: 11B11, 10 μg ml^{-1}) were added to media, and for T_h2 differentiation, murine IL-4 (10 ng ml^{-1}) and anti-mouse IFN-γ (clone: XMG 1.2, 10 μg ml^{-1}) were added. Cells were cultured with cytokines alone for another 2–3 days in six-well plate (4 ml per well), harvested and treated with Ficoll-Paque™ PLUS (#17-1440-02; GE Healthcare, Buckinghamshire, UK) to isolate live cells and washed thoroughly. T_h1- or T_h2-polarlized cells were re-stimulated with immobilized anti-CD3ε mAb (1 μg ml^{-1} for coating) and cytokines (IL-2: 100 U ml^{-1}, IL-18: 100 ng ml^{-1}) at 1×10^6 cells ml^{-1} in 24-well plate (1 ml per well).

Intracellular staining of cytokines and transcription factors

Cytokine staining and transcription factor staining were carried out using Fixation and Permeabilization Kit (88-8823-88;

eBioscience) and Foxp3 Staining Buffer Set (00-5523-00; eBioscience), respectively, according to manufacturer's instruction.

Real-time PCR analysis

Total RNA was extracted with TRIzol solution (15596-018; Invitrogen, Carlsbad, CA, USA) and treated with DNase I (18068-015; Invitrogen) to digest residual genomic DNA. Reverse transcription was performed using an iScript cDNA Synthesis Kit (170-8891; BioRad Laboratories, Hercules, CA, USA) according to manufacturer's instruction. Primers and probes of TaqMan® Gene Expression Assays for Gata3 (Mm01337569_m1), Il13 (Mm00434204_m1), and Actb (Mm00607939_s1) were purchased from Applied Biosystems (Foster City, CA, USA). The levels of *Gata3* and *Il13* mRNA were normalized to *Actb* mRNA.

Chromatin Immunoprecipitation assay

Chromatin immunoprecipitation (ChIP) assay was performed as described previously (22). Immunoprecipitated DNA was quantified by real-time PCR, and results were normalized to input DNA. Sequences of primers used in the analysis were described previously (23).

Transfection of small interfering RNA

Stealth™ RNAi Negative Universal Control (#12935-400) and Stealth™ small interfering RNA (siRNA) specific for Gata3 (set of three oligos) (#1320003) were purchased from Invitrogen. On day 5 of T_h differentiation, 1×10^7 T_h1 cells were transfected with siRNA (1 nmol per transfection). For transfection, Nucleofector II module (Lonza, Basel, Switzerland) was used together with Mouse T cell Kit (VPA-1006; Lonza) under the control of program X-001. After transfection, cells were cultured with 100 U ml^{-1} recombinant human IL-2 in mouse T-cell media supplied by Mouse T cell Kit for 12 h. Live cells were isolated through Ficoll-Paque™ PLUS treatment and re-stimulated with plate-bound anti-CD3ε (1 μg ml^{-1} for coating) plus cytokines for 24 h.

Statistical analysis

All data are presented as mean and SD and statistical analysis was performed using the Student's *t*-test. Differences were recognized as significant with a P value of <0.05.

Results

IL-18 stimulation reciprocally regulates IFN-γ and IL-13 production by T_h1 cells stimulated with anti-CD3 and IL-2

In our previous report, we demonstrated that in response to OVA and IL-2, OVA-specific T_h1 cells or T_h2 cells produced IFN-γ or IL-4/IL-13, respectively, and that additional IL-18 stimulation induced OVA-activated T_h1 cells to increase IFN-γ production and to start IL-13 production (5).

Here, we primed naive $CD4^+$ T cells derived from wild-type BALB/c spleens by culturing them with anti-CD3 and anti-CD28 antibodies under T_h1 or T_h2 cell-skewing condition. Upon challenge with anti-CD3 and IL-2, T_h1 and T_h2 cells produce IFN-γ and IL-4/IL-13, respectively (Fig. 1A). In contrast, upon challenge with anti-CD3 and IL-18 or anti-CD3, IL-2 and IL-18, T_h1 cells not only increased IFN-γ production but also started IL-13 production (Fig. 1A). Furthermore, when stimulated with anti-CD3 and IL-18 or anti-CD3, IL-2 and IL-18 for 72 h, T_h1 cells strongly increased IL-13 production (Fig. 1B). As additional IL-2 stimulation failed to augment IL-13 production by anti-CD3 plus IL-18-stimulated T_h1 cells (Fig. 1A and B), we suspected that anti-CD3 plus IL-18-stimulated T_h1 cells simultaneously produced sufficient IL-2.

We next examined the proportion of T_h1 cells producing IL-13 and/or IFN-γ by flow cytometry (Fig. 1C). T_h1 cells or T_h2 cells were induced *in vitro* followed by challenge with anti-CD3 and IL-2. T_h1 and T_h2 cells produce IFN-γ and IL-4, respectively (Fig. 1C, left panel). We parallel stimulated T_h1 cells or T_h2 cells by culturing with anti-CD3 and IL-2 or with anti-CD3, IL-2 and IL-18 for 24–72 h (Fig. 1C, right panel). T_h1 cells stimulated with anti-CD3 plus IL-2 modesty developed into IL-13-producing cells or IFN-γ plus IL-13-producing cells (Fig. 1C, right panel). In contrast, T_h1 cells additionally stimulated with IL-18 strongly developed into IL-13-producing cells or IL-13 plus IFN-γ-producing super T_h1 cells and at the same time diminished their development into IFN-γ-producing cells (Fig. 1C, right panel), suggesting a reciprocal effect of IL-18 on IL-13 and IFN-γ production. In contrast, T_h2 cells strongly produced IL-13 in response to anti-CD3 and IL-2 (Fig. 1C, right panel). As expected from these results, T_h1 cells strongly increased *Il13* mRNA expression in response to anti-CD3, IL-2 and IL-18 (Fig. 1D). Taken together, IFN-γ-producing cells seem to develop into IL-13-producing cells via super T_h1 stage, or directly into IL-13-producing cells, and IL-13 production by T_h1 cells stimulated with additional IL-18 is regulated at the level of *Il13* transcription.

T_h1 cells increase Gata3 gene expression when stimulated with anti-CD3, IL-2 and IL-18

Because Gata3 is known as a master regulator for T_h2 differentiation and has the crucial role of regulating T_h2 cytokine gene expression (24–27), we focused on Gata3 expression in super T_h1 cells. T_h1 cells and T_h2 cells were stimulated with anti-CD3 and IL-2 in the presence or absence of IL-18 for 12 or 24 h and *Gata3* mRNA expression was assessed by real-time PCR. As expected, T_h1 cells increased *Gata3* mRNA in response to stimulation with anti-CD3 and IL-2 or anti-CD3, IL-2 and IL-18 (Fig. 2A). We next tested whether T_h1 cells indeed increased their expression of Gata3 protein. As IL-18Rα is a useful T_h1 cell marker (28), we stained T_h1 or T_h2 cells with fluorochrome-conjugated anti-IL-18Rα, anti-Gata3 and anti-T-bet antibodies and analysed them by flow cytometry (Fig. 2B). As reported elsewhere, most T_h2 cells lacked IL-18Rα and T-bet but strongly expressed Gata3 protein. In contrast, T_h1 cells expressed IL-18Rα and T-bet but mostly lacked Gata3. However, consistent with the results of *Gata3* mRNA expression (Fig. 2A), IL-18Rα-expressing T_h1 cells increased the proportion of cells positive for Gata3 at 24 h after stimulation with anti-CD3 and IL-2 (Fig. 2B). Additional IL-18 stimulation markedly increased the proportion of T_h1 cells positive for Gata3 and more than 70% of IL-18Rα-expressing T_h1 cells co-expressed T-bet and Gata3

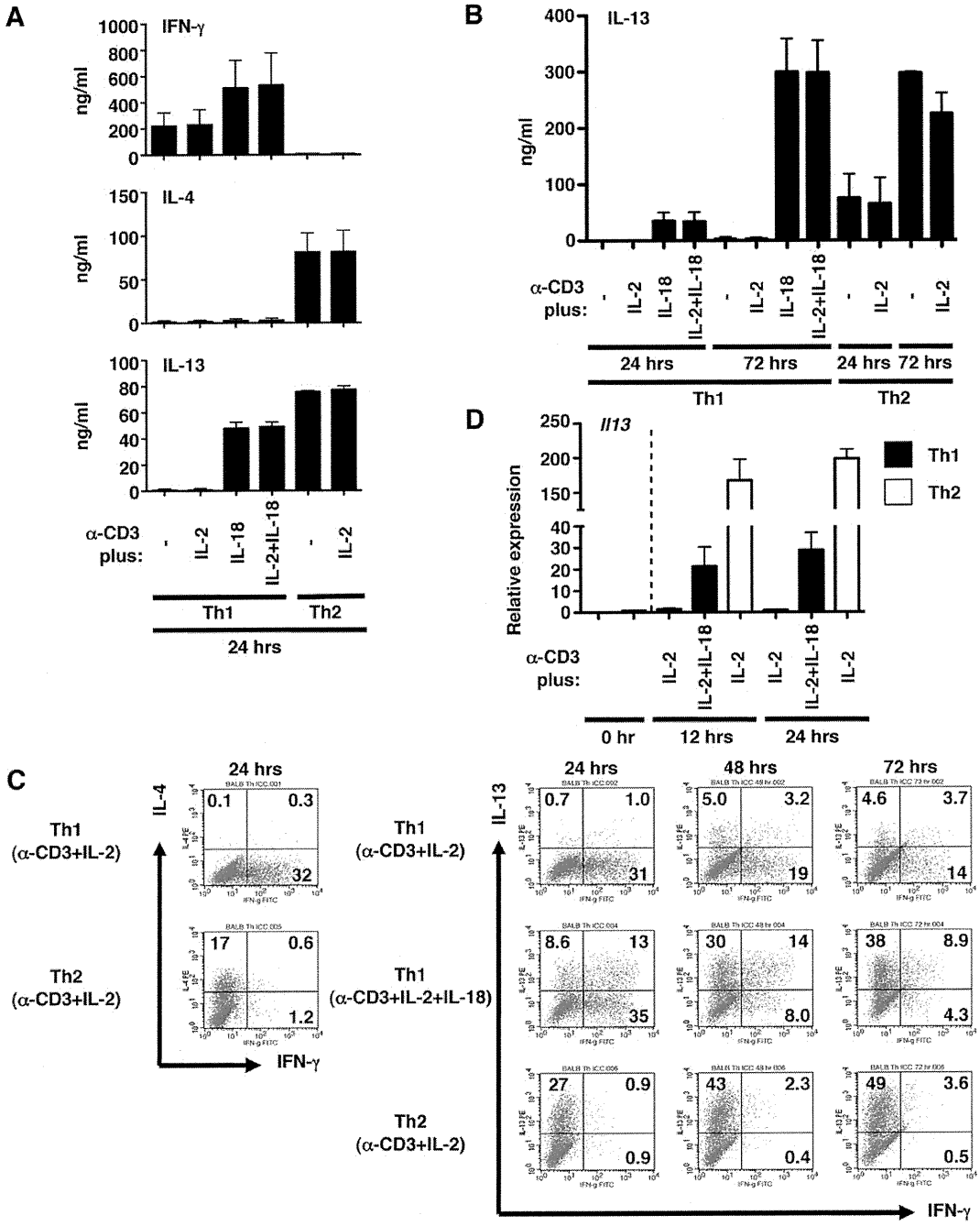

Fig. 1. Simultaneous production of IFN-γ and IL-13 from T_h1 cells in response to TCR, IL-2 and IL-18. (A, B) T_h1 cells simultaneously produce IFN-γ and IL-13 in response to anti-CD3, IL-2 and IL-18. Naive $CD4^+$ T cells from wild-type BALB/c mice were primed with anti-CD3 and anti-CD28 antibodies and differentiated under T_h1 or T_h2 conditions for 5 days. T_h1 or T_h2 cells were challenged with anti-CD3 plus the indicated cytokines for 24–72 h. Culture supernatants were subjected to ELISA measurement. (C) Proportion of T_h1 cells producing IL-13 and/or IFN-γ. T_h1 or T_h2 cells were challenged with anti-CD3 plus the indicated cytokines and subjected to intracellular cytokine staining. (D) T_h1 cells increase *Il13* mRNA in response to anti-CD3, IL-2 and IL-18. T_h1 or T_h2 cells were re-stimulated with anti-CD3 plus cytokines as indicated. Total RNA from these cells was reverse-transcribed to cDNA followed by real-time PCR analysis on *Il13* expression. Data are representative of two independent experiments with similar results (C) and indicate the mean of two independent experiments (A, B, D).

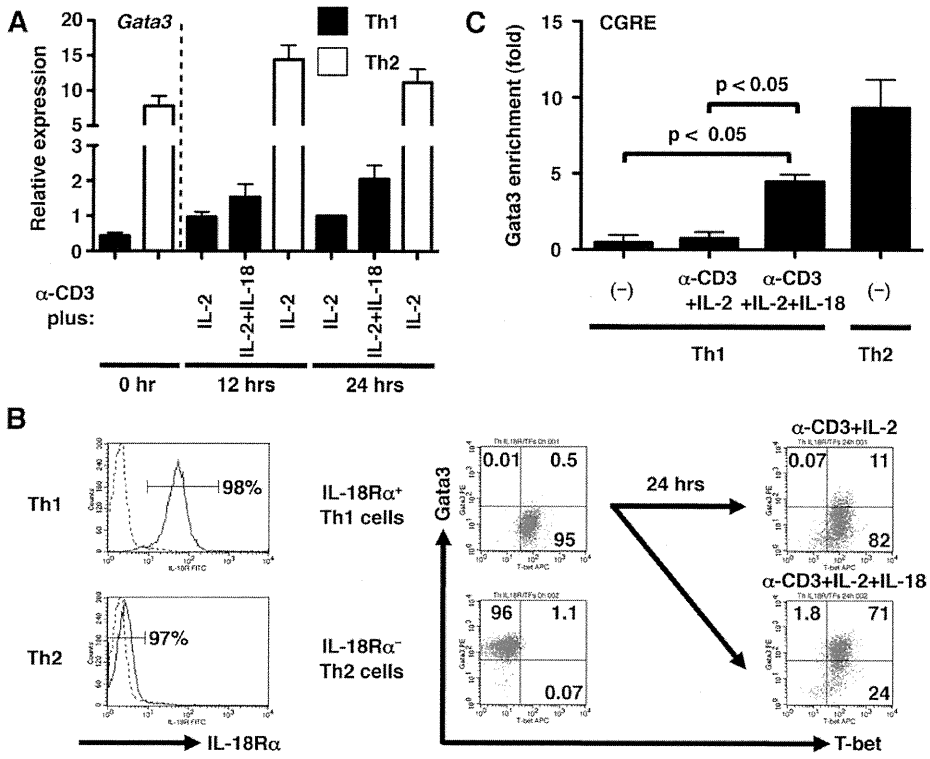

Fig. 2. T_h1 cells increase *Gata3* expression when stimulated with anti-CD3, IL-2 and IL-18. (A) *Gata3* expression in super T_h1 cells is regulated at the level of transcription. cDNA used in Fig. 1(D) was subjected to real-time PCR analysis on *Gata3* expression. (B) Additional IL-18 stimulation increases the proportion of cells positive for Gata3 in T-bet-expressing T_h1 cells. T_h1 and T_h2 cells re-stimulated as indicated were stained with anti-mouse IL-18Rα (clone: Y38) followed by FITC-conjugated anti-rat IgG_1, PE-conjugated anti-Gata3 and Alexa Fluor® 647-conjugated anti-T-bet antibodies. The expression of IL-18Rα, Gata3 and T-bet protein was assessed by flow cytometry. (C) Gata3 binds to CGRE containing nucleosome in super T_h1 cells. T_h1 cells were pre-treated with anti-FasL antibody (2 μg ml^{-1}) for 1 h and re-stimulated with anti-CD3 plus cytokines as indicated in the presence of anti-FasL antibody (1 μg ml^{-1}) for 24 h. The extent of Gata3 binding to the CGRE motif on *Il13* gene was evaluated by ChIP assay. Immunoprecipitated DNA was quantified by real-time PCR, and results were normalized to input DNA. Data are representative of two independent experiments with similar results (B) and indicate the mean of two independent experiments (A, C).

(Fig. 2B), suggesting that IL-18 is required for co-expression of T-bet and Gata3. Together, these results indicate that stimulation with anti-CD3, IL-2 and IL-18 induces T_h1 cells to develop into IL-13-producing cells or IL-13 plus IFN-γ-producing cells primarily by increasing Gata3 expression, without affecting T-bet expression level.

Contribution of Gata3 to Il13 gene expression

There is a conserved Gata3 response element (CGRE) 1.6-kb upstream of the *Il13* gene (22). Gata3 binds to the CGRE motif, which is a potent enhancer in the regulation of *Il13* transcription (23). Thus, we examined binding of Gata3 to the CGRE motif on the *Il13* gene in T_h1 cells by ChIP assay (Fig. 2C). To obtain enough viable T_h1 cells after re-stimulation, we added anti-FasL mAb before and during incubation to reduce apoptosis. Treatment with anti-FasL antibody did not affect *Gata3* and *Il13* mRNA expression in T_h1 cells (Supplementary Figure 1, available at *International Immunology* Online). As reported previously, we could detect Gata3 protein binding to the CGRE motif on the *Il13* gene in T_h2 cells but very little in T_h1 cells. However, in correlation well with results shown in Fig. 2(B), we could detect Gata3 protein binding to the CGRE motif on the *Il13* gene in T_h1 cells only after stimulation with anti-CD3, IL-2 and IL-18 (Fig. 2C). Taken together, these results imply that induction of Gata3 and binding of Gata3 to the CGRE motif in T_h1 cells required IL-18 co-stimulation and that Gata3 induction and Gata3 binding to CGRE motif are critical for the induction of *Il13* expression in super T_h1 cells.

IL-4 is required for Gata3 expression in T_h1 cells

Gata3 gene expression in T_h2 cells is positively regulated by stimulation with TCR, IL-2 and IL-4 (27). In particular, an IL-4R-mediated signaling pathway is critical for *Gata3* gene expression in T_h2 cells. Thus, we compared IL-4Rα expression by T_h1 cells and T_h2 cells. A large fraction of IL-18Rα-expressing T_h1 cells expressed IL-4Rα with relatively lower mean fluorescence intensity (Fig. 3A). In contrast, T_h2 cells lacking IL-18Rα have a lager proportion of IL-4Rα-positive cells with relatively higher mean fluorescence intensity (Fig. 3A). Thus, to examine the contribution of IL-4Rα to *Gata3* expression in T_h1 cells, we stimulated T_h1 cells with anti-CD3, IL-2 and IL-18 in the absence or presence of anti-IL-4Rα antibody. Anti-IL-4Rα antibody treatment blocked this induction

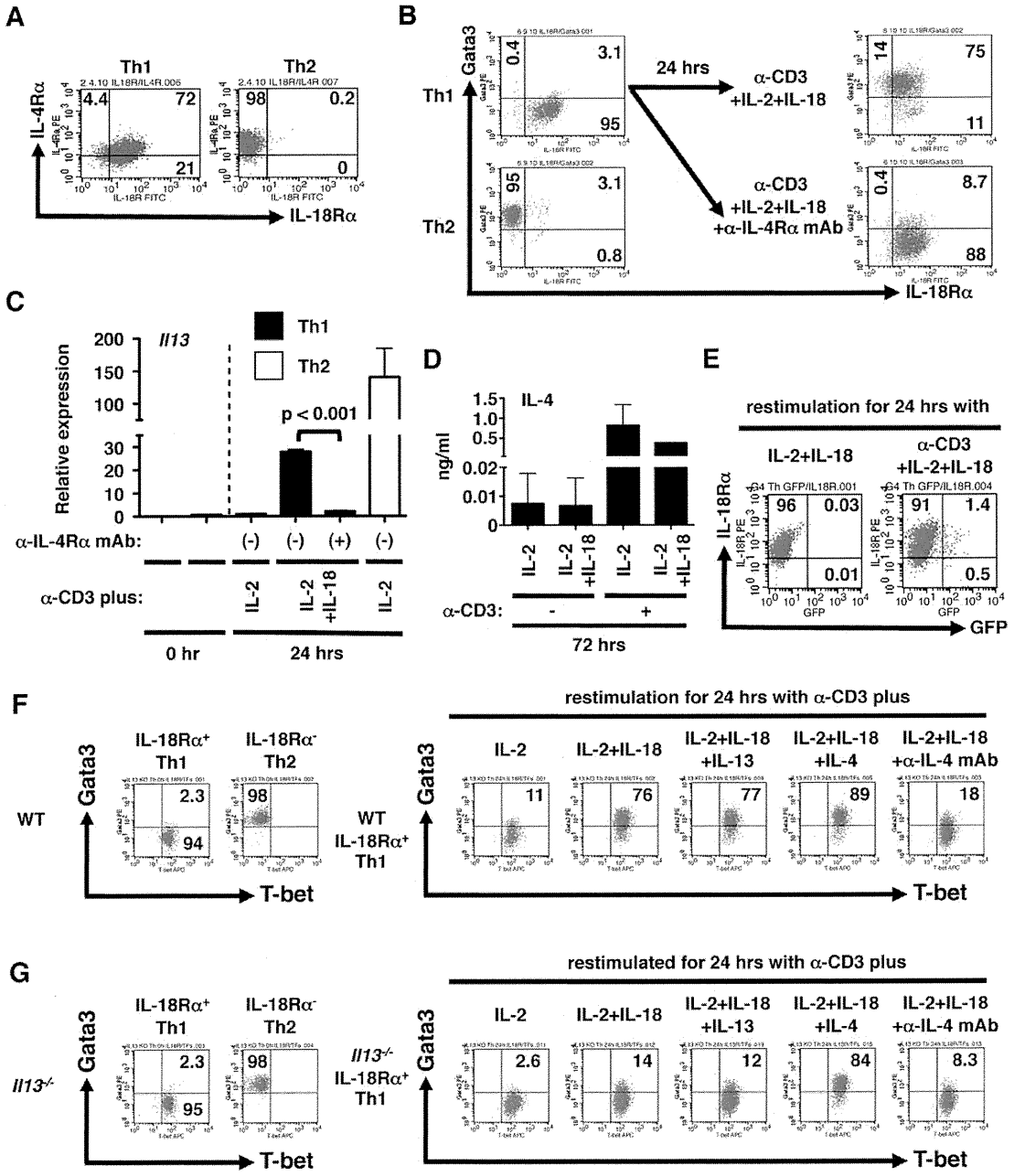

Fig. 3. Requirement of IL-4 for *Gata3* gene expression in super T_h1 cells. (A) T_h1 cells express both IL-18Rα and IL-4Rα. After differentiation for 5 days, T_h1 or T_h2 cells were stained with FITC-conjugated anti-IL-18Rα (clone: 112614) and PE-conjugated anti-IL-4Rα antibodies and analysed by flow cytometry. (B, C) IL-4Rα signaling pathway contributes to *Il13* gene expression through Gata3 induction in super T_h1 cells. T_h1 cells were pre-treated with anti-IL-4Rα antibody or isotype control (20 μg ml^{-1}) for 1.5 h and re-stimulated with anti-CD3 plus indicated cytokines in the presence of anti-IL-4Rα antibody (10 μg ml^{-1}) or isotype control for 24 h. Cells were stained with FITC-conjugated anti-mouse IL-18Rα (clone: 112614) and PE-conjugated anti-Gata3 antibodies (B). Total RNA from these cells was reverse transcribed to cDNA followed by real-time PCR analysis on *Il13* expression (C). (D) T_h1 cells produce small but significant amount of IL-4. T_h1 cells were re-stimulated as indicated for 72 h. Culture supernatants were subjected to ELISA measurement. (E) Anti-CD3 stimulation induces IL-4 production by IL-18Rα$^+$ T_h1 cells. *Il4*$^{gfp/gfp}$ T_h1 cells were re-stimulated as indicated for 24 h and stained with anti-mouse IL-18Rα (clone: Y38) followed by biotin-conjugated anti-rat IgG_1 and Streptoavidin-PE. (F) Contribution of IL-4 to *Gata3* expression in super T_h1 cells. C57BL/6 T_h1 cells were re-stimulated as indicated for 24 h and stained with anti-mouse IL-18Rα (clone: Y38) followed by FITC-conjugated anti-rat IgG_1, PE-conjugated anti-Gata3 and Alexa Fluor® 647-conjugated anti-T-bet antibodies. The expression of IL-18Rα, Gata3 and T-bet protein was assessed by flow cytometry. (G) Defect of Gata3 induction in *Il13*$^{-/-}$ T_h1 cells is rescued by additional IL-4, but not IL-13. *Il13*$^{-/-}$ T_h1 cells were re-stimulated as indicated for 24 h. The expression

of Gata3-positive cells (Fig. 3B) and significantly decreased *Il13* mRNA expression (Fig. 3C), suggesting that IL-4Rα signaling pathway contributes to *Il13* gene expression through Gata3 induction in super T_h1 cells.

We next examined which cytokine activates IL-4Rα signaling pathway in T_h1 cells. By ELISA measurement, we confirmed that T_h1 cells produced small but significant amount of IL-4 when stimulated with anti-CD3 plus IL-2, whereas IL-18 co-stimulation failed to increase IL-4 production by T_h1 cells in the presence and absence of anti-CD3 stimulation (Fig. 3D). To formally prove that anti-CD3 stimulation induces IL-4 production by IL-18Rα-expressing T_h1 cells, we differentiated naive $CD4^+$ T cells from $Il4^{gfp/gfp}$ mice (20) harboring a green fluorescent protein (GFP) gene inserted to *Il4* allele, into T_h1 cells, and monitored GFP expression in response to stimulation with anti-CD3, IL-2 and IL-18. We found that these T_h1 cells express GFP (Fig. 3E), confirming that T_h1 cells (1.4%) produce IL-4 in response to anti-CD3, IL-2 and IL-18. Thus, to examine the contribution of IL-4 to Gata3 induction, we stimulated T_h1 cells with anti-CD3, IL-2 and IL-18 in the presence of exogenous IL-4 and anti-IL-4 antibody and monitored Gata3 expression (Fig. 3F). More than 70% of IL-18Rα-expressing T_h1 cells expressed Gata3 after stimulation with anti-CD3, IL-2 and IL-18 (Fig. 3F, right panel). Exogenous IL-4 stimulation modestly up-regulated Gata3 induction and anti-IL-4 antibody treatment markedly decreased this induction of Gata3-positive cells (Fig. 3F, right panel), suggesting the contribution of IL-4 to *Gata3* expression in super T_h1 cells.

IL-4Rα plays a key role in the binding affinity of both IL-13R and IL-4R complexes (29). Thus, to examine the positive feedback loop between Gata3 induction and IL-13 production by super T_h1 cells, we employed wild-type and $Il13^{-/-}$ T_h1 cells. The profile of T-bet and Gata3 expression in $Il13^{-/-}$ T_h1 cells and T_h2 cells was similar to that of wild-type cells (Fig. 3F, left panel and Fig. 3G, left panel). However, after re-stimulation, IL-4 production by $Il13^{-/-}$ T_h1 cells was very modest and that by $Il13^{-/-}$ T_h2 cells was also relatively smaller than that of wild-type cells (Supplementary Figure 2, available at *International Immunology* Online). We suspect that the insertion of a neomycin resistance gene to *Il13* locus might negatively regulate *Il4* gene by changing chromatin structure of adjacently located *Il4* locus. In parallel with decreased IL-4 production by $Il13^{-/-}$ T_h1 cells, the proportion of Gata3-positive cells was markedly reduced in $Il13^{-/-}$ T_h1 cells after stimulation with anti-CD3, IL-2 and IL-18 (Fig. 3G, right panel). The defect of Gata3 induction was rescued by exogenous IL-4 stimulation but not exogenous IL-13 stimulation (Fig. 3G, right panel). These finding suggests that IL-4 binding to IL-4R complex activates *Il13* gene expression by up-regulating Gata3 induction in super T_h1 cells.

Stat6, NFAT and NF-κB are responsible for Gata3 gene expression insuper T_h1 cells

Stat6 is a critical transcription factor in IL-4R signaling (19, 30) and IL-4-induced Stat6 activation is a crucial event in *Gata3* gene expression during T_h2 differentiation (27, 31). To examine the role of Stat6 in *Gata3* expression in super T_h1 cells, we employed wild-type and $Stat6^{-/-}$ T_h1 cells for real-time PCR analysis. $Stat6^{-/-}$ T_h1 cells failed to express *Gata3* mRNA when stimulated with anti-CD3, IL-2 and IL-18, and exogenous IL-4 could not rescue the defect of *Gata3* expression in $Stat6^{-/-}$ T_h1 cells (Fig. 4A), suggesting that Stat6 regulates *Gata3* expression. In parallel with reduced *Gata3* expression, the proportion of IL-13-producing cells and IFN-γ plus IL-13-producing cells was markedly reduced in $Stat6^{-/-}$ T_h1 cells after stimulation with anti-CD3, IL-2, IL-18 and IL-4 (Supplementary Figure 2, available at *International Immunology* Online). Thus, endogenous IL-4 derived from anti-CD3 plus IL-2-stimulated T_h1 cells induced Stat6 activation, which in turn synergizes with other transcription factors to induce Gata3 expression in T_h1 cells stimulated with anti-CD3 and IL-18. NFAT and NF-κB are known as key transcription factors downstream of TCR and IL-18R, respectively, and both supposedly activate *Gata3* gene transcription (1, 27, 32). Treatment with NFAT inhibitor or NF-κB inhibitor APDC inhibited *Gata3* expression in T_h1 cells stimulated with anti-CD3, IL-2 and IL-18, even if exogenous IL-4 was added to the culture to exclude the potential inhibitory effect of these inhibitors on IL-4 production (Fig. 4B). Taken together, these results indicate that anti-CD3-induced NFAT activation, IL-4-induced Stat6 activation and IL-18-induced NF-κB activation synergistically induce *Gata3* gene expression in super T_h1 cells (33).

Gata3 is a critical transcription factor to induce Il13 gene expression in T_h1 cells

Next, to test the requirement for Gata3 on *Il13* gene activation in T_h1 cells, we transfected T_h1 cells with 'scrambled' control siRNA or experimental siRNA nucleotide to deplete *Gata3* mRNA. The cells were rested for 12 h after transfection and re-stimulated with anti-CD3, IL-2 and IL-18 for 24 h. To exclude its potent inhibitory effect on IL-4 production, IL-4 was provided to the culture exogenously and abundantly. Compared to control siRNA, transfection of Gata3-specific siRNA dramatically reduced the proportion of Gata3-positive cells without affecting IL-18Rα expression (Fig. 5A). Flow cytometry showed that reduction of Gata3-positive cells by Gata3-specific siRNA resulted in diminution of IL-13-producing cells and IFN-γ plus IL-13-producing cells and simultaneous up-regulation of IFN-γ-producing cells (Fig. 5B), suggesting that Gata3 directly regulates *Il13* gene activation in T_h1 cells stimulated with anti-CD3, IL-2 and IL-18 independently of IL-4 production.

Gata3 is essential but not sufficient for IL-13 production

In this report, we show that Gata3 is required for *Il13* gene expression in super T_h1 cells (Fig. 5) and that *Gata3* gene expression is induced by IL-4 released from T_h1 cells after anti-CD3 stimulation (Fig. 3). To investigate the relationship between anti-CD3 stimulation, Gata3 induction and IL-13 production, we stimulated T_h1 cells with IL-2, IL-2 plus IL-4, IL-2

of IL-18Rα, Gata3 and T-bet protein was assessed by flow cytometry. Data are representative of two independent experiments with similar results (A, B, E, F, G) and indicate the mean of two independent experiments (C, D).

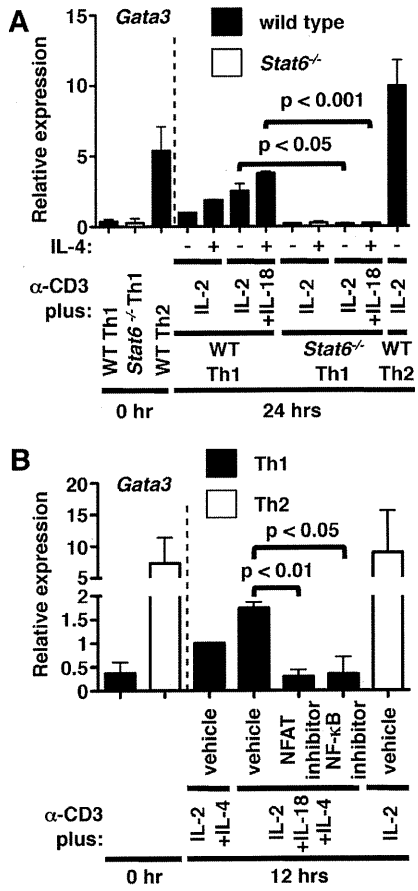

Fig. 4. Stat6, NFAT and NF-κB are involved in *Gata3* gene expression in super T_h1 cells. (A) Involvement of Stat6 in *Gata3* gene expression in super T_h1 cells. Wild-type BALB/c and *Stat6*$^{-/-}$ T_h1 or T_h2 cells were re-stimulated as indicated for 24 h. Exogenous IL-4 was added at 10 ng ml^{-1}. cDNA was subjected to real-time PCR analysis on *Gata3* expression. (B) Involvement of NFAT and NF-κB in *Gata3* gene expression in super T_h1 cells. T_h1 cells were pre-treated with NFAT inhibitor (100 μM) and NF-κB inhibitor (APDC) (10 μM) for 2 h to inhibit NFAT and NF-κB activation, respectively, and re-stimulated as indicated for 12 h in the presence of these inhibitors. Exogenous IL-4 was supplemented at 10 ng ml^{-1} to exclude the potential effect of these inhibitors on endogenous IL-4 production. Data indicate the mean of two independent experiments (A, B).

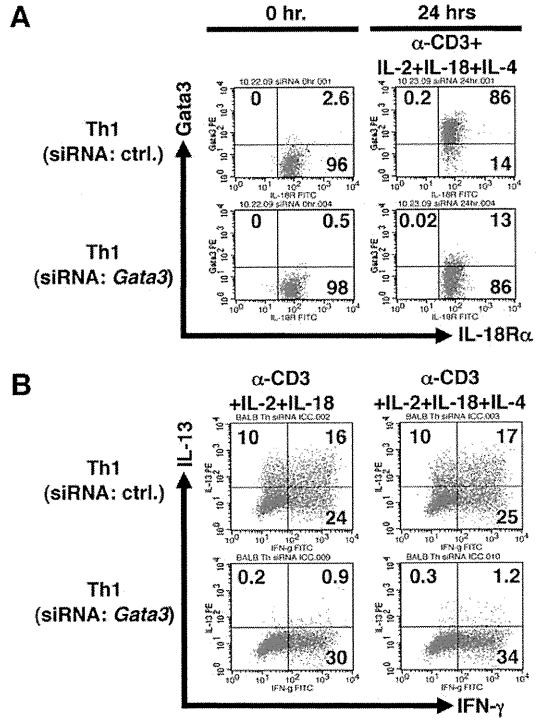

Fig. 5. Gata3 is a critical transcription factor for *Il13* gene activation in super T_h1 cells. (A) Reduced proportion of Gata3-positive cells in T_h1 cells by transfection of Gata3-specific siRNA. T_h1 cells were transfected with scrambled control siRNA or Gata3-specific siRNA and rested for 12 h. Live cells were re-stimulated as indicated (exogenous IL-4: 10 ng ml^{-1}) for 24 h and stained with anti-mouse IL-18Rα (clone: Y38) followed by FITC-conjugated anti-rat IgG_1 and PE-conjugated anti-Gata3 antibodies. (B) Reduction of IL-13-producing and IFN-γ plus IL-13-producing cells by Gata3-specific siRNA. After re-stimulation for 24 h, cells were subjected to intracellular cytokine staining as indicated. Data are representative of two independent experiments with similar results (A, B).

plus IL-18 or IL-2 plus IL-18 plus IL-4 in the presence or absence of anti-CD3 stimulation and monitored Gata3 induction and IL-13 production by flow cytometry (Fig. 6). In the presence of anti-CD3 stimulation (Fig. 6A), which induces endogenous IL-4 production by T_h1 cells (Fig. 4D and E), T_h1 cells strongly increased the proportion of cells positive for Gata3 in response to IL-2 and IL-18 and additional IL-4 stimulation only modestly enhanced this proportion (Fig. 6A, upper panel). In agreement with Gata3 expression level, anti-CD3-stimulated T_h1 cell markedly increased the proportion of IL-13-producing cells and IFN-γ plus IL-13-producing cells in response to IL-2 plus IL-18 or IL-2, IL-18 and IL-4 (Fig. 6A, lower panel). In contrast, in the absence of anti-CD3 stimulation, T_h1 cells strongly increased their proportion of Gata3-positive cells only when stimulated with IL-2, IL-18 and IL-4 (Fig. 6B, upper panel). However, these T_h1 cells could not produce IL-13 (Fig. 6B, lower panel), although we could detect Gata3 protein binding to the CGRE motif on the *Il13* gene in T_h1 cells after stimulation with IL-2, IL-18 and IL-4 by ChIP assay (Fig. 6C). Thus, we could speculate that such Gata3-expressing T_h1 cells start to produce IL-13 upon anti-CD3 challenge. As speculated, T_h1 cells pre-treated with IL-2, IL-18 and IL-4 successfully increased their proportion of IL-13-producing and IFN-γ plus IL-13-producing cells in response to anti-CD3 plus IL-2 (Fig. 6D). Based on these results, we conclude that Gata3 induction prepares T_h1 cells to produce IL-13 promptly in response to TCR engagement.

Discussion

Recently, we have demonstrated that IL-13 production by super T_h1 cells is a major event in the pathogenesis of infection-induced allergic disorders (5–10). However, the mechanism underlying IL-13 production by super T_h1 cells has not been elucidated.

In this report, we reveal that Gata3 transcription factor is absolutely required for *Il13* expression in super T_h1 cells.

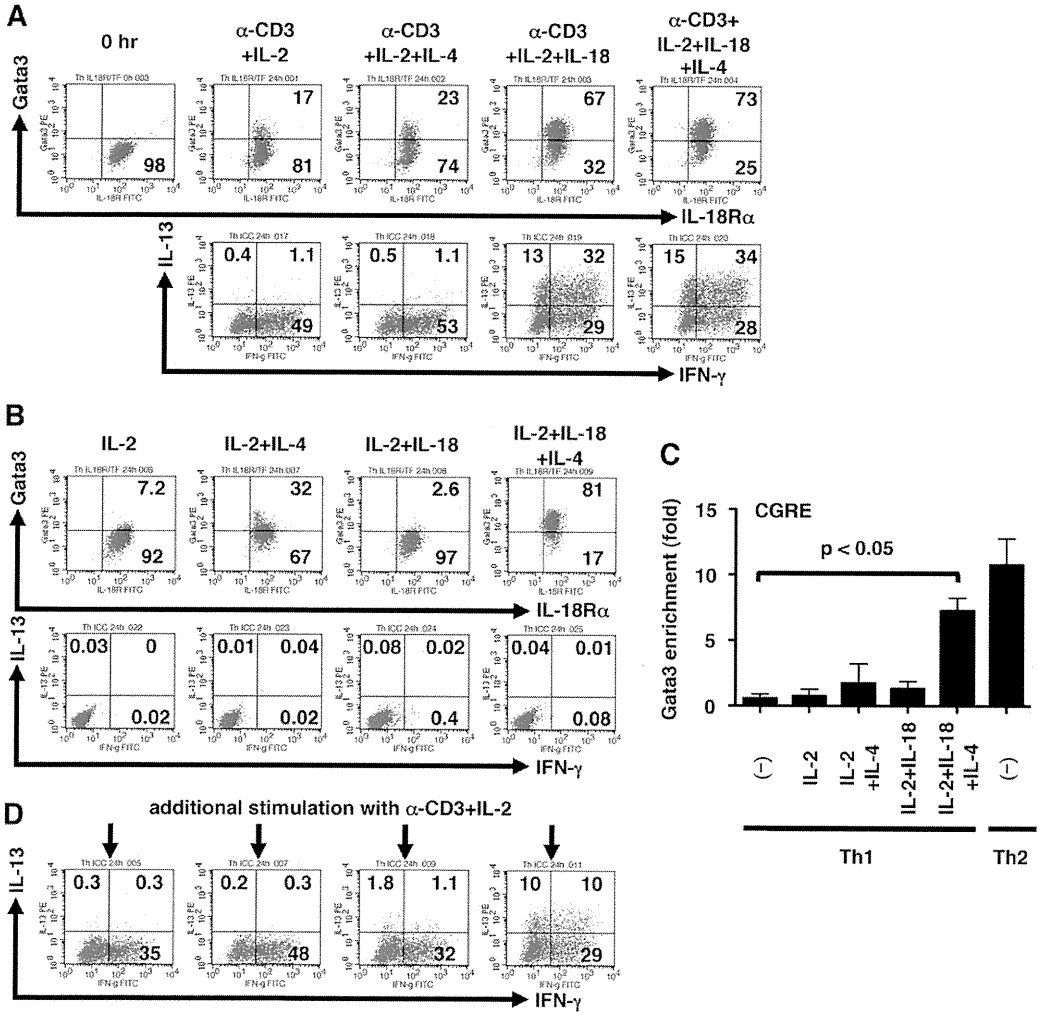

Fig. 6. Gata3 is essential but not sufficient for IL-13 production in super T_h1 cells. (A) Correlation of Gata3 expression level with IL-13 production by T_h1 cells in the presence of TCR signaling. T_h1 cells were stimulated with cytokines in the presence of anti-CD3 (1.0 μg ml^{-1}) as indicated for 24 h. Cells were stained with anti-mouse IL-18Rα (clone: Y38) followed by FITC-conjugated anti-rat IgG_1 and PE-conjugated anti-Gata3 antibodies or with fluorochrome-conjugated anti-cytokine antibodies. (B) Gata3-expressing T_h1 cells fail to produce IL-13 in the absence of TCR signaling. T_h1 cells were stimulated with cytokines as indicated in the absence of anti-CD3 for 24 h and subjected to intracellular staining. (C) Gata3 binds to the CGRE motif on the *Il13* gene in T_h1 cells stimulated with IL-2, IL-18 and IL-4 in the absence of anti-CD3. After stimulation with cytokines as indicated for 24 h, the extent of Gata3 binding to the CGRE motif on *Il13* gene was evaluated by ChIP assay. Immunoprecipitated DNA was quantified by real-time PCR, and results were normalized to input DNA. (D) TCR signaling is required to start IL-13 production by Gata3-expressing T_h1 cells. T_h1 cells shown in Fig. 6(B) were further stimulated with anti-CD3 and IL-2 for 24 h and subjected to intracellular cytokine staining. Data are representative of two independent experiments with similar results (A, B, D) and indicate the mean of two independent experiments (C).

Gata3 is synergistically induced by transcription factors including NFAT, NF-κB and Stat6, which are activated by TCR engagement, IL-18 stimulation and IL-4 stimulation, respectively, and functions by binding to the CGRE motif on the *Il13* gene. We found that Gata3 induction is essential but not satisfactory for *Il13* gene expression in super T_h1 cells. As we demonstrated, TCR engagement is simultaneously needed to induce IL-13 production by Gata3-expressing IL-2, IL-18 and IL-4-stimulated T_h1 cells.

IL-2-stimulated T_h1 cells increased Gata3 expression weakly when stimulated with IL-4, while they strongly increased Gata3 expression when additionally stimulated with IL-18 (Fig. 6B, upper panel). Besides, we could detect Gata3 binding to the CGRE motif on *Il13* gene in T_h1 cells stimulated with IL-2, IL-18 and IL-4 (Fig. 6C). Thus, TCR engagement is not required for Gata3 binding, although TCR engagement is essential for IL-13 production (Fig. 6D). TCR engagement is essential for at least two reasons. One is that it is required for IL-4 production by T_h1 cells. Another is that it is required for NFAT activation, which is critically involved in triggering *Il13* gene expression in Gata3-expressing T_h1 cells. In addition to them, TCR engagement might contribute to stability of Gata3 protein as

TCR-activated Ras-ERK MAPK cascade stabilizes Gata3 protein in T_h2 cells (34).

Recently, Motomura *et al.* (35) showed considerable enrichment of histone H3 trimethylation at Lys4 in the hypersensitive (HS) 1 region of the *Il13* promoter even in T_h1 cells, suggesting that the *Il13* promoter is transcriptionally accessible even in T_h1 cells as well as T_h2 cells. In accordance with their observation, in the present report, we demonstrate that Gata3 protein, which is induced by stimulation with IL-2, IL-18 and IL-4 in T_h1 cells, can bind to the *Il13* CGRE motif even in the absence of TCR stimulation (Fig. 6B and C). However, Gata3 binding to the CGRE motif is not satisfactory and TCR engagement is simultaneously needed to induce IL-13 production by Gata3-expressing T_h1 cells (Fig. 6D). To date, recent reports have revealed that IL-13 production by T_h2 cells is determined by promoter-related regulation rather than epigenetic regulation (23, 35). For example, using targeted deletion of a series of DNase I–HS sites located *Il4-Il13* locus in mice, Tanaka *et al.* (23) demonstrated that Gata3 directly activates the *Il13* promoter in T_h2 cells through its binding to the CGRE motif, whereas its binding to HS2 regulates chromatin modification on the *Il4* locus. Motomura *et al.* (35) suggested that the transcription factor E4BP4 (E4 promoter-binding protein 4) regulates *Il13* gene expression in chronically antigen-stimulated T_h1 cells by activating *Il13* promoter. Thus, we speculate that *Il13* gene expression in super T_h1 cells might be regulated by two distinct classes of transcription factors through promoter/enhancer-mediated mechanism: Gata3 activates an *Il13* gene enhancer by binding to the CGRE motif and TCR-activated transcription factors such as NFAT finally triggers *Il13* gene transcription by activating *Il13* gene promoter (Supplementary Figure 4, available at *International Immunology* Online).

Although *Il4* and *Il13* loci are adjacent to each other on murine chromosome 11 or human chromosome 5, super T_h1 cells produce abundant IL-13 but little IL-4 (Fig. 1). In contrast, T_h2 cells co-upregulate production of both cytokines. Besides, we demonstrate that additional IL-18 stimulation strongly induced IL-13 production in anti-CD3-stimulated T_h1 cells and incubation period dependently diminished IFN-γ production (Fig. 1C). We could speculate that co-expression of T-bet and Gata3 (Fig. 2B) induces this unique cytokine profile of super T_h1 cells. T-bet with Runx3 directly participates in *Il4* silencing by binding to HS4 in T_h1 cells (36, 37). Gata3 is involved in the induction of transcriptionally permissive chromatin structure in *Il4* gene locus during T_h2 differentiation and *Il4* gene locus is transcriptionally repressive in T_h1 cells. For *Il13* transcription in T_h2 cells, Gata3 functions as an enhancer by binding to the CGRE motif on *Il13* gene (22, 23). Thus, T-bet expressed in super T_h1 cells suppresses *Il4* gene and transcriptionally repressive chromatin structure in *Il4* gene locus, which is established during T_h1 differentiation, might be sustained in T_h1 cells even after Gata3 induction. When Gata3 is induced in T-bet-expressing T_h1 cells stimulated with anti-CD3, IL-2 and IL-18, Gata3 could directly bind to the CGRE motif on the *Il13* gene, resulting in simultaneous production of IL-13 and IFN-γ at 24 h. However, when T-bet-expressing T_h1 cells are stimulated with anti-CD3, IL-2 and IL-18 much longer, Gata3 begins to contribute to silencing *Ifng* gene by binding to the *Ifng* promoter, resulting in diminution of IFN-γ production by T_h1 cells (38). At present, we only have the data that Gata3 binds to the CGRE motif on the *Il13* gene even in the presence of abundant T-bet. We need further study to define the mechanism for reciprocal effect of IL-18 on IL-13 and IFN-γ production.

Recently, Hegazy *et al.* (18) revealed that T_h1 cell-inducing cytokines together with TCR stimulation can induce T-bet expression in T_h2 cells by demonstrating that when stimulated with LCMV $GP_{61–68}$ epitope, IL-12, IFN-γ and type I interferons, T_h2 cells can be reprogrammed into $Gata3^+T\text{-}bet^+$ cells capable of producing both IL-4 and IFN-γ. In this report, we revealed that IL-4, T_h2 cell-inducing cytokine, has the ability to allow even T-bet-expressing T_h1 cells to co-express Gata3 (Figs 2 and 3). *In vivo* observations have shown that T_h1 and T_h2 cells co-exist with each other. For example, a small but significant population of IFN-γ- or IL-4-producing $CD4^+$ T cells can be detected even in T_h2- or T_h1-skewing condition such as helminth or protozoa infection, respectively. Thus, these findings imply that under the circumstances in which T_h1 cells and T_h2 cells co-exist, these cells might act on each other to modify the function of the other party. In addition to T_h2 cells, several types of cells can possibly become the source of IL-4 to induce the development of super T_h1 cells. Basophils and mast cells derived from bone marrow cells cultured with IL-3 express IL-18R and IL-33R and produce T_h2 cytokines including IL-4 in response to stimulation with IL-3 and IL-18 or IL-33 without FcεRI cross-link (39). Basophils produce IL-4 by incubating with IL-3 plus antigen or by capturing antigen-IgE complex (40–42). Moreover, IL-18 with IL-2 promotes T_h2 cytokine production including IL-4 from T cells and NKT cells (43, 44). We need further study to manifest the condition in which super T_h1 cells are spontaneously generated from T_h1 cells.

Because the number of naive $CD4^+$ T cells is gradually reduced with age, the plasticity of T_h cells could contribute to host defense by developing immune responses to newly encountered pathogens. However, under these circumstances, the plasticity of T_h cells also participates in the onset of allergic diseases, as we have demonstrated that the development of super T_h1 cells from T_h1 cells is involved in microbial infection-associated allergic diseases such as bronchial asthma and atopic dermatitis. In agreement with these findings, distinct from 'classical' T_h2-type allergy seen in children, infection-induced (T_h1 type) allergic diseases are often observed in adult people. Thus, the acquisition of the plasticity in cytokine expression by T_h cells is associated with both efficient immune responses and the pathogenesis of infection-induced allergic disorders.

Supplementary data

Supplementary Figures 1– 4 are available at *International Immunology* Online.

Funding

Ministry of Education, Culture, Sports, Science, and Technology of Japan [Grants-in-Aid for Young Scientists (B) (20790379 and 22790476 to M.N.), Grants-in-Aid for Scientific Research on Priority Areas (18073016 to K.N.) and Hitech Research Center Grant (to K.N.)]; Japan Society for the Promotion of Science [Grants-in-Aid for Scientific

Research (20390145 and 19390121 to K.N.)]; Japanese Ministry of Health, Labor and Welfare (Grants for Research on Emerging and Re-emerging Infectious Diseases to K.N.).

Acknowledgements

We are very grateful to Dr William E. Paul (National Institutes of Health/ National Institute of Allergy and Infectious Diseases) for critical comments on the manuscript.

References

1 Ansel, K. M., Djuretic, I., Tanasa, B. and Rao, A. 2006. Regulation of Th2 differentiation and Il4 locus accessibility. *Annu. Rev. Immunol.* 24:607.
2 Amsen, D., Spilianakis, C. G. and Flavell, R. A. 2009. How are T(H)1 and T(H)2 effector cells made? *Curr. Opin. Immunol.* 21:153.
3 Wilson, C. B., Rowell, E. and Sekimata, M. 2009. Epigenetic control of T-helper-cell differentiation. *Nat. Rev. Immunol.* 9:91.
4 Zhu, J., Yamane, H. and Paul, W. E. 2010. Differentiation of effector CD4 T cell populations. *Annu. Rev. Immunol.* 28:445.
5 Sugimoto, T., Ishikawa, Y., Yoshimoto, T., Hayashi, N., Fujimoto, J. and Nakanishi, K. 2004. Interleukin 18 acts on memory T helper cells type 1 to induce airway inflammation and hyperresponsiveness in a naive host mouse. *J. Exp. Med.* 199:535.
6 Hata, H., Yoshimoto, T., Hayashi, N., Hada, T. and Nakanishi, K. 2004. IL-18 together with anti-CD3 antibody induces human Th1 cells to produce Th1- and Th2-cytokines and IL-8. *Int. Immunol.* 16:1733.
7 Hayashi, N., Yoshimoto, T., Izuhara, K., Matsui, K., Tanaka, T. and Nakanishi, K. 2007. T helper 1 cells stimulated with ovalbumin and IL-18 induce airway hyperresponsiveness and lung fibrosis by IFN-gamma and IL-13 production. *Proc. Natl Acad. Sci. USA* 104:14765.
8 Terada, M., Tsutsui, H., Imai, Y. *et al.* 2006. Contribution of IL-18 to atopic-dermatitis-like skin inflammation induced by *Staphylococcus aureus* product in mice. *Proc. Natl Acad. Sci. USA* 103:8816.
9 Nakanishi, K., Tsutsui, H. and Yoshimoto, T. 2010. Importance of IL-18-induced super Th1 cells for the development of allergic inflammation. *Allergol. Int.* 59:137.
10 Kuroda-Morimoto, M., Tanaka, H., Hayashi, N. *et al.* 2010. Contribution of IL-18 to eosinophilic airway inflammation induced by immunization and challenge with *Staphylococcus aureus* proteins. *Int. Immunol.* 22:561.
11 Zhou, L., Chong, M. M. and Littman, D. R. 2009. Plasticity of CD4+ T cell lineage differentiation. *Immunity* 30:646.
12 Zhu, J. and Paul, W. E. 2009. Heterogeneity and plasticity of T helper cells. *Cell. Res* 20:4.
13 Murphy, K. M. and Stockinger, B. 2010. Effector T cell plasticity: flexibility in the face of changing circumstances. *Nat. Immunol.* 11:674.
14 O'Shea, J. J. and Paul, W. E. 2010. Mechanisms underlying lineage commitment and plasticity of helper CD4+ T cells. *Science* 327:1098.
15 Lee, Y. K., Turner, H., Maynard, C. L. *et al.* 2009. Late developmental plasticity in the T helper 17 lineage. *Immunity* 30:92.
16 Oldenhove, G., Bouladoux, N., Wohlfert, E. A. *et al.* 2009. Decrease of Foxp3+ Treg cell number and acquisition of effector cell phenotype during lethal infection. *Immunity* 31:772.
17 Wei, G., Wei, L., Zhu, J. *et al.* 2009. Global mapping of H3K4me3 and H3K27me3 reveals specificity and plasticity in lineage fate determination of differentiating CD4+ T cells. *Immunity* 30:155.
18 Hegazy, A. N., Peine, M., Helmstetter, C. *et al.* 2010. Interferons direct Th2 cell reprogramming to generate a stable GATA-3(+)T-bet(+) cell subset with combined Th2 and Th1 cell functions. *Immunity* 32:116.
19 Kaplan, M. H., Schindler, U., Smiley, S. T. and Grusby, M. J. 1996. Stat6 is required for mediating responses to IL-4 and for development of Th2 cells. *Immunity* 4:313.
20 Hu-Li, J., Pannetier, C., Guo, L. *et al.* 2001. Regulation of expression of IL-4 alleles: analysis using a chimeric GFP/IL-4 gene. *Immunity* 14:1.
21 McKenzie, G. J., Emson, C. L., Bell, S. E. *et al.* 1998. Impaired development of Th2 cells in IL-13-deficient mice. *Immunity* 9:423.
22 Yamashita, M., Ukai-Tadenuma, M., Kimura, M. *et al.* 2002. Identification of a conserved GATA3 response element upstream proximal from the interleukin-13 gene locus. *J. Biol. Chem.* 277:42399.
23 Tanaka, S., Motomura, Y., Suzuki, Y. *et al.* 2011. The enhancer HS2 critically regulates GATA-3-mediated Il4 transcription in T(H)2 cells. *Nat. Immunol.* 12:77.
24 Pai, S. Y., Truitt, M. L. and Ho, I. C. 2004. GATA-3 deficiency abrogates the development and maintenance of T helper type 2 cells. *Proc. Natl Acad. Sci. USA* 101:1993.
25 Yamashita, M., Ukai-Tadenuma, M., Miyamoto, T. *et al.* 2004. Essential role of GATA3 for the maintenance of type 2 helper T (Th2) cytokine production and chromatin remodeling at the Th2 cytokine gene loci. *J. Biol. Chem.* 279:26983.
26 Zhu, J., Min, B., Hu-Li, J. *et al.* 2004. Conditional deletion of Gata3 shows its essential function in T(H)1-T(H)2 responses. *Nat. Immunol.* 5:1157.
27 Ho, I. C., Tai, T. S. and Pai, S. Y. 2009. GATA3 and the T-cell lineage: essential functions before and after T-helper-2-cell differentiation. *Nat. Rev. Immunol.* 9:125.
28 Yoshimoto, T., Takeda, K., Tanaka, T. *et al.* 1998. IL-12 up-regulates IL-18 receptor expression on T cells, Th1 cells, and B cells: synergism with IL-18 for IFN-gamma production. *J. Immunol.* 161:3400.
29 Andrews, A. L., Holloway, J. W., Holgate, S. T. and Davies, D. E. 2006. IL-4 receptor alpha is an important modulator of IL-4 and IL-13 receptor binding: implications for the development of therapeutic targets. *J. Immunol.* 176:7456.
30 Takeda, K., Tanaka, T., Shi, W. *et al.* 1996. Essential role of Stat6 in IL-4 signalling. *Nature* 380:627.
31 Ouyang, W., Löhning, M., Gao, Z. *et al.* 2000. Stat6-independent GATA-3 autoactivation directs IL-4-independent Th2 development and commitment. *Immunity* 12:27.
32 Das, J., Chen, C. H., Yang, L., Cohn, L., Ray, P. and Ray, A. 2001. A critical role for NF-kappa B in GATA3 expression and TH2 differentiation in allergic airway inflammation. *Nat. Immunol.* 2:45.
33 Shen, C. H. and Stavnezer, J. 1998. Interaction of stat6 and NF-kappaB: direct association and synergistic activation of interleukin-4-induced transcription. *Mol. Cell. Biol.* 18:3395.
34 Yamashita, M., Shinnakasu, R., Asou, H. *et al.* 2005. Ras-ERK MAPK cascade regulates GATA3 stability and Th2 differentiation through ubiquitin-proteasome pathway. *J. Biol. Chem.* 280:29409.
35 Motomura, Y., Kitamura, H., Hijikata, A. *et al.* 2011. The transcription factor E4BP4 regulates the production of IL-10 and IL-13 in CD4+ T cells. *Nat. Immunol.* 12:450.
36 Ansel, K. M., Greenwald, R. J., Agarwal, S. *et al.* 2004. Deletion of a conserved Il4 silencer impairs T helper type1-mediated immunity. *Nat. Immunol.* 5:1251.
37 Djuretic, I. M., Levanon, D., Negreanu, V., Groner, Y., Rao, A. and Ansel, K. M. 2007. Transcription factors T-bet and Runx3 cooperate to activate Ifng and silence Il4 in T helper type 1 cells. *Nat. Immunol.* 8:145.
38 Chang, S. and Aune, T. M. 2007. Dynamic changes in histone-methylation 'marks' across the locus encoding interferon-gamma during the differentiation of T helper type 2 cells. *Nat. Immunol.* 8:723.
39 Yoshimoto, T., Tsutsui, H., Tominaga, K. *et al.* 1999. IL-18, although antiallergic when administered with IL-12, stimulates IL-4 and histamine release by basophils. *Proc. Natl Acad. Sci. USA* 96:13962.
40 Perrigoue, J. G., Saenz, S. A., Siracusa, M. C. *et al.* 2009. MHC class II-dependent basophil-CD4+ T cell interactions promote T(H)2 cytokine-dependent immunity. *Nat. Immunol.* 10:697.
41 Yoshimoto, T., Yasuda, K., Tanaka, H. *et al.* 2009. Basophils contribute to T(H)2-IgE responses *in vivo* via IL-4 production and presentation of peptide-MHC class II complexes to CD4+ T cells. *Nat. Immunol.* 10:706.